

CBPF - CENTRO BRASILEIRO DE PESQUISAS FÍSICAS

Rio de Janeiro

Monografia

CBPF-MO-001/86

MODELS IN ELEMENTARY PARTICLE PHYSICS*

by

W. Majerotto

Centro Brasileiro de Pesquisas Físicas - CNPq/CBPF
Rua Dr. Xavier Sigaud, 150
22290 - Rio de Janeiro, RJ - Brasil

Permanent address: Institute for High Energy Physics of the
Austrian Academy of Sciences, Vienna, Austria.

* Lectures given at Centro Brasileiro de Pesquisas Físicas during September
and October 1985.



CNPq - Conselho Nacional de Desenvolvimento Científico e Tecnológico

CONTENTS

| | <u>Page</u> |
|---|-------------|
| 1. Introduction - The Standard Model | 1 |
| 1.1 - The building blocks of matter | 1 |
| 1.2 - Forces - gauge bosons | 2 |
| 1.3 - The gauge symmetry SU(2)xU(1)xSU(3)..... | 2 |
| 1.4 - The SU(2)xU(1)xSU(3) structure of fermions | 3 |
| 1.5 - Colour | 5 |
| 1.6 - Evidence for quarks | 5 |
| 1.7 - Masses | 6 |
| 1.8 - Still many unsolved problems | 7 |
| 2. Basics of QCD | 8 |
| 2.1 - Basic couplings..... | 8 |
| 2.2 - Effective coupling constant $\alpha_s(Q^2)$ -Asymptotic free - dom | 9 |
| 2.3 - Applications | 12 |
| 3. Testing QCD in $e^+e^- \rightarrow$ hadrons | 13 |
| 3.1 - The simple quark picture | 13 |
| 4. Effects of QCD - $O(\alpha_s)$ corrections, 3 jet events | 16 |
| 4.1 - The total cross section | 16 |
| 4.2 - The gluon jet: $e^+e^- \rightarrow q\bar{q}g$ | 17 |
| 4.3 - Jet measures | 21 |
| 5. Deep inelastic lepton-hadron scattering | 22 |
| 5.1 - Kinematics | 22 |
| 5.2 - Quark-parton model | 24 |
| 5.2.1 - Electron scattering | 25 |
| 5.2.2 - Neutrino scattering | 31 |
| 5.3 - Influence of gluons (QCD effects) | 34 |

| | <u>page</u> |
|---|-------------|
| 6. Large p_T processes in hadron-hadron scattering - jets at the collider | 39 |
| 6.1 - The general picture | 39 |
| 6.2 - Basic mechanism | 40 |
| 6.3 - Angular distribution | 44 |
| 6.4 - Structure functions, factorization | 45 |
| 7. Drell-Yan Process | 47 |
| 7.1 - QCD-effects | 49 |
| 8. W-Z Physics | 51 |
| 8.1 - W-Z Production | 51 |
| 8.2 - Detection of $W \rightarrow e(\mu)+\nu$ | 54 |
| 8.3 - Charge asymmetry in $W \rightarrow e\nu$ | 56 |
| 8.4 - The quark structure functions | 57 |
| 8.5 - Comparison with the predictions by the Standard Model | 59 |
| 9. Hadronization of quarks and gluons | 66 |
| 9.1 - The fragmentation function | 67 |
| 9.2 - The Independent Fragmentation Model (IFM) | 70 |
| 9.3 - The Lund String Model | 74 |
| 9.4 - Parton Shower Models | 78 |
| 9.5 - Gluon versus quark jets | 80 |
| 10. Soft Hadronic Interactions | 80 |

1. Introduction - The Standard Model

Due to extensive experimental and theoretical efforts within the last two decades a comprehensive picture of elementary particle physics has emerged. It is therefore called the "Standard Model". As we shall see, it is still incomplete in many respects. But there is at present no experimental fact which is in contradiction with it either.

1.1. The building blocks of matter

Within this picture the building blocks of all matter are spin $\frac{1}{2}$ fermions: quarks and leptons. They are pointlike particles (at least down to a distance of $\sim 10^{-16}$ cm). They appear in 3 families as shown in Table 1.

| | Particles | | | Q | Forces |
|---------|-----------|-----------|------------|------|--|
| Leptons | ν_e | ν_μ | ν_τ | 0 | only weak |
| | e | μ | τ | -1 | weak and electromagnetic |
| Quarks | u | c | $t^?$ | 2/3 | weak, electromagnetic and strong |
| | d | s | b | -1/3 | |

Table 1

Here u, d, c, s, t, b denote the up, down, charm, strange, top, and bottom quark, respectively, i.e. the 6 quark flavours. There is not yet any clear experimental evidence for the existence of the top quark although data from the UA1 $\bar{p}p$ collider experiment at CERN may indicate a signal in the mass range of $30 \leq m_t \leq 50$ GeV. The properties of

ν_τ neutrinos are inferred from decays. So far no reaction induced by a ν_τ has been observed.

1.2. Forces - Gauge Bosons

The three types of forces between these fermions, the weak, electromagnetic and strong force, are described by a local gauge symmetry of the underlying Lagrangian. The forces are then mediated by gauge bosons i.e. spin 1 bosons, the weak force by the intermediate vector bosons W^+ , W^- , Z^0 the electromagnetic force by the photon γ , and the strong force by 8 gluons. The electromagnetic force is of infinite range due to the massless photon ($V(r) \sim \frac{1}{r}$). The weak force has short range ($\sim 10^{-15}$ cm) because the W^\pm and Z^0 have a large mass (see below) ($V(r) \sim \frac{e^{-Mr}}{r}$). Although the gluons are assumed to be massless the strong force is of finite range (~ 1 fm) because the nature of the force is believed to confine the quarks within the size of nucleons. This confinement mechanism, which is not yet fully understood, is presumably also the reason why one has never found a free quark.

1.3. The gauge symmetry $SU(2) \times U(1) \times SU(3)$

The essential point of the "Standard Model" is the underlying gauge symmetry $SU(2)_W \times U(1)_Y \times SU(3)_C$, see Table 2.

| Local gauge symmetry | Gauge bosons | |
|-----------------------|-----------------------------|---|
| $SU(2)_W$ $U(1)_Y$ | W^+, W^-, Z^0 γ | Electroweak Theory (Glashow-Weinberg-Salam Model) |
| $SU(3)_C$ | 8 gluons | Quantum Chromodynamics (QCD) theory of strong interactions |

Table 2

The first two parts, $SU(2)_W \times U(1)_Y$, describe electromagnetic and weak interactions. Here $SU(2)_W$ refers to the weak isospin I_W and has 3 generators $(\tau_i, i = 1, 2, 3)$ to which there correspond 3 vector bosons W^+, W^-, W^0 . $U(1)_Y$ has one generator corresponding to the weak hypercharge Y , where $Q = I_3^W + Y$. It implies one gauge boson B . The photon and the Z^0 are then orthogonal components of W^0 and B . We know that the symmetry $SU(2) \times U(1)$ must be broken at low energies (< 100 GeV) where only the electromagnetic part $U(1)_{\text{elm}}$ is exact.

The second row (in Table 2), corresponds to $SU(3)_C$, the symmetry of quantum chromodynamics (QCD), which is the best candidate for describing strong interactions, $SU(3)_C$ refers to the three colour charges, for instance, r(ed), b(lue), g(reen), $SU(3)_C$ has 8 generators $(\lambda_i, i = 1, \dots, 8, \text{the so called Gell-Mann matrices})$ and therefore gives rise to 8 gauge bosons, the gluons.

1.4. The $SU(2) \times U(1) \times SU(3)$ structure of fermions

Each fermion family has the properties with respect to the symmetry as shown in Table 3 (only for the first generation):

| | | | I_3^W | Y |
|--|---|------------------------------|-------------|-----------------|
| $\begin{pmatrix} \nu_e \\ e \end{pmatrix}_L$ | $\begin{pmatrix} u \\ d' \end{pmatrix}_L^{r,b,g}$ | $\leftarrow SU(2)_W$ doublet | 1/2 -1/2 | $Y = Q - I_3^W$ |
| e_R | $u_R^{r,b,g}, d_R^{r,b,g}$ | $\leftarrow SU(2)_W$ singlet | 0 0 | |
| $SU(3)_C$ - singlet [†] | $SU(3)_C$ - triplets [†] (3 colours) | | | |

Table 3

Here e_L and e_R denote the left- and right-handed electron, respectively. u_R, d_R, u_L, d_L have analogous meanings.

There is a subtlety in the model: the mass eigenstates d, s, b , are superpositions of the "weak eigenstates" d', s', b' where

$$\begin{pmatrix} d' \\ s' \\ b' \end{pmatrix} = U \begin{pmatrix} d \\ s \\ b \end{pmatrix}, \quad U = (3 \times 3) \text{ matrix} \\ \text{(Kobayashi-Maskawa matrix)}$$

The matrix U contains 3 angles and 1 phase, the latter being responsible for CP-violation as seen in K^0 decays. We have approximately $|U_{11}| \approx |U_{22}| \approx \cos \theta_c = 0.97$, $|U_{12}| \approx |U_{21}| \approx \sin \theta_c \approx 0.23$, $|U_{23}| \approx |U_{32}| = 0.05$, $|U_{33}| \approx 1$, $|U_{13}| \approx |U_{31}| \approx 0$.

It is interesting to note that the association of quarks and leptons into one family is essential. In order to guarantee the theory to be "anomaly free" (and renormalizable) the sum of the charges of all fundamental fermions must vanish, i.e.,

$$Q_e + Q_\nu + 3(Q_u + Q_d) = 0$$

The factor 3 stems from the 3 colours. The relation is fulfilled by each generation.

1.5. Colour

Colour is the crucial quantum number of $SU(3)_c$ (strong interactions). On the other hand coloured quarks or gluons have never been directly observed. It is therefore worthwhile to look for evidence for 3 "colours". For example, the $\pi^0 \rightarrow 2\gamma$ decay turns out to be too small by a factor of 9 without colour. By introducing colour one was able to solve a paradox in the "old" quark picture. The Δ^{++} -resonance consists of three u quarks, all with their spins parallel (and in relative s-waves) to make a spin 3/2 state with no angular momentum. Such a completely symmetric state is however forbidden by Fermi statistics. Only by introducing a new quantum number (colour) for quarks, i.e., by describing Δ^{++} as a state $u^r u^g u^b$ is it possible to solve the problem. Perhaps the strongest evidence for colour comes from measuring the cross section ratio

$$R = \frac{\sigma(e^+e^- \rightarrow \gamma^* \rightarrow \text{hadrons})}{\sigma(e^+e^- \rightarrow \mu^+\mu^-)} \approx 3 \sum_q e_q^2$$

where e_q is the charge of the quarks involved. It is again this factor 3 which is needed to explain the data. We shall come back to this point later.

1.6. Evidence for quarks

Although it seems most likely that quarks do not exist as free particles, we have

clear evidence for their existence mainly coming from e^+e^- annihilation, deep inelastic lepton-hadron reactions, as well as from hard (high p_T) processes in hadron-hadron collisions. This will be discussed in detail in the next lectures. Quarks and gluons manifest themselves as hadron jets which have been clearly seen in e^+e^- annihilation as well as in $\bar{p}p$ reactions at the CERN collider. In particular the three jet events are an evidence for the existence of gluons.

1.7. Masses

Since free quarks are not seen, it is a priori not clear what the mass of a quark is. The masses entering the QCD Lagrangian are the "current" masses which are felt through weak and electromagnetic currents. They are: $m_u = 5\text{MeV}$, $m_d = 9\text{MeV}$, $m_s = 175\text{MeV}$, $m_c = 1.25\text{ GeV}$, $m_b \approx 4.5\text{ GeV}$, $m_t = 40\text{ GeV}$ (?). The u, d and s quark masses are therefore negligible whereas the c, b, t quarks are called heavy quarks. We need not mention that the quark masses are not yet understood.

The most recent values for the mass of the W and the Z^0 are (Bari Conf. 1985)

$$M_W = 83.1 \begin{array}{l} + 1.3 \\ - 0.8 \end{array} \pm 3. \text{ GeV} \quad (\text{UA1})$$

$$\quad \quad \quad (\text{stat.}) \quad (\text{sys.})$$

$$= 81.2 \pm 1.1 \pm 1.3 \text{ GeV} \quad (\text{UA2})$$

$$M_Z = 93.0 \pm 1.6 \pm 3. \text{ GeV} \quad (\text{UA1})$$

$$= 92.5 \pm 1.3 \pm 1.5 \text{ GeV} \quad (\text{UA2})$$

(They agree beautifully with the Standard Model prediction:

$$M_W = 82.2 \pm 1.8 \text{ GeV}, \quad M_Z = 93.2 \pm 0.02 \text{ GeV}.$$

Local gauge invariance would require all the gauge bosons to be massless. The masses of the vector bosons are generated by the so called Higgs mechanism.

To be more precise, the Lagrangian remains invariant (necessary for the renormalizability) but the ground state ("vacuum") breaks the symmetry ("spontaneous symmetry breaking"). In order to give the vector bosons a mass it is necessary to introduce a new field (spin 0) associated to the Higgs particle H^0 . This has not yet been found. Its mass is expected to lie between 10 GeV and 1 TeV.

1.8. Still many unsolved problems

Despite the consistency and the beautiful agreement with experiment the "Standard Model" leaves many questions open:

- Why are there three families ?

There cannot be many more. Astrophysics tells us that the number of neutrinos N_ν must be ≤ 4 . The collider experiment UA1 and UA2 conclude that $(N_\nu - 3) \leq 2.4 \pm 1.0$ (90% C.L.)

- The model does not represent a complete unification of all interactions including gravity. Even without the latter the simplest scheme SU(5) does not work due to the recent experimental bounds for the proton decay. (SU(5) predicts $\tau_p = 3.2 \times 10^{29 \pm \frac{2.1}{2.5}}$ ys whereas according to experiment $\tau_p > 10^{31}$ ys).

Moreover, we have

- No real understanding of the masses

- Too many parameters

- no real understanding of the Higgs mechanism in addition to the fact that the Higgs particle has not yet been found.

2. Basics of QCD

2.1 - Basic couplings:

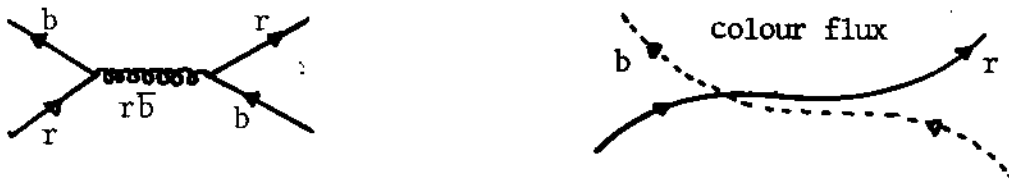
The strong interaction takes place between coloured quarks and massless coloured gluons. More precisely the gluon carries colour-anti-colour. Thus a gluon can be in 8 different colour combinations

$$r\bar{g}, r\bar{b}, g\bar{r}, g\bar{b}, b\bar{r}, b\bar{g}, \frac{1}{\sqrt{2}} (r\bar{r}-g\bar{g}), \frac{1}{\sqrt{6}} (r\bar{r} + g\bar{g} - 2b\bar{b})$$

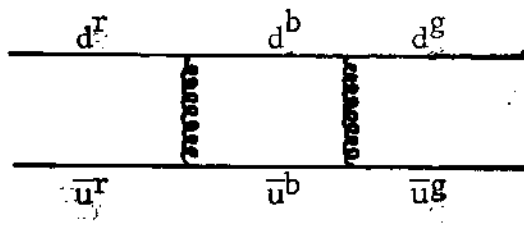
i.e., the gluons belong to an SU(3) colour octet.

The remaining combination $\frac{1}{\sqrt{3}} (r\bar{r}+g\bar{g} + b\bar{b})$ is an SU(3) singlet and therefore does not have colour and cannot mediate between coloured quarks.

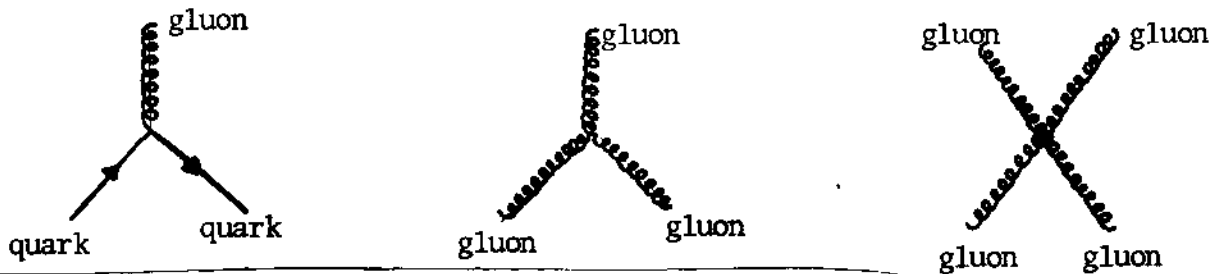
For instance one can have the following interaction



A pion being $\pi^- \sim \sum_{\text{colour}} \bar{u}_i d_i$ can be imagined



The basic couplings in QCD are

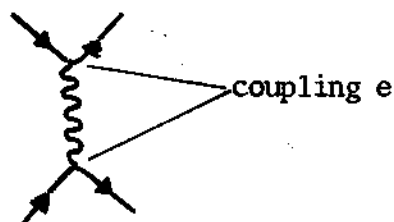


whereas the first two graphs are of the order g_s (g_s is the strong coupling constant) the third is proportional to g_s^2 .

Note that gluon can couple to itself via the three and the four gluon couplings. This is a characteristic feature of the non-Abelian nature of QCD and is not present in QED.

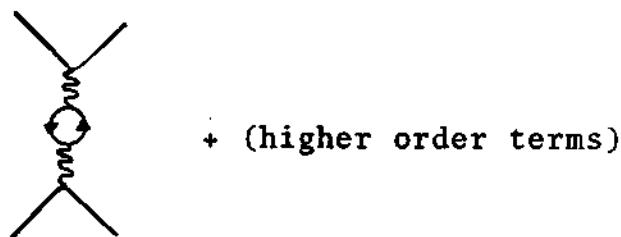
2.2. Effective coupling constant $\alpha_s(Q^2)$ -Asymptotic freedom

Let us compare with QED. If we want to measure the coupling e or $\alpha^2 = e^2/4\pi$ we can do electron-electron scattering:



where the photon exchanged has a momentum squared $q^2 = -Q^2$, $Q^2 > 0$.

We however know that the photon propagator is modified by the vacuum polarization, i.e., we have to include the diagrams



This leads to the following behaviour of the coupling (in leading order)

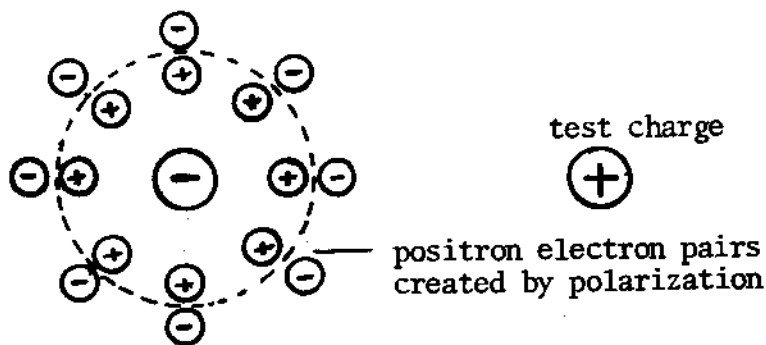
$$\alpha(Q^2) \approx \alpha(\mu^2) \left[1 + \frac{\alpha(\mu^2)}{3\pi} \log \frac{Q^2}{\mu^2} + \dots \right]$$

where μ is the arbitrary normalization point at which α has been measured, for instance $\alpha(m_e^2) = 1/137$.

Actually one has in the brackets a geometrical series, and by summing it up one gets

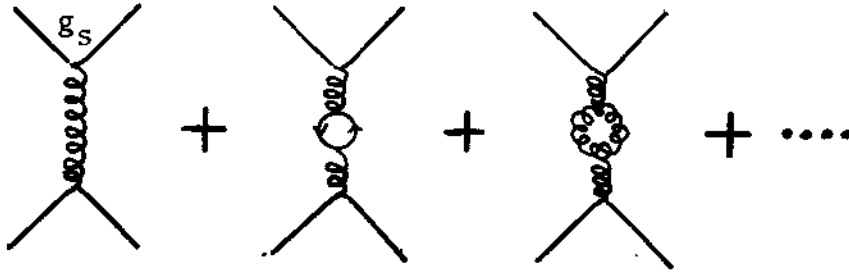
$$\alpha(Q^2) \approx \frac{\alpha(\mu^2)}{1 - \frac{\alpha(\mu^2)}{3\pi} \log \frac{Q^2}{\mu^2}} \quad \text{for } Q^2 \gg \mu^2 \quad (2.1)$$

We thus have effectively a "running" coupling constant which changes with Q^2 . The coupling becomes bigger as Q^2 increases or when going to smaller distances. The dependence is of course very weak. This phenomenon can be understood by the "charge screening". Let us measure the charge of the electron by a positive test charge as shown in the figure



If the test charge is far away we see the electron surrounded by positrons screening the electron's charge. If we however come very close to the electron we penetrate this cloud of positrons and feel a larger charge.

Now let us turn to the QCD case. In an analogous way we have to calculate the following graphs:



The lines are now quarks and the curled lines gluons. We then arrive at the following result (in leading order)

$$\alpha_s(Q^2) = \frac{g_s^2}{4\pi} = \frac{\alpha(\mu^2)}{1 + \frac{b_0}{4\pi} \alpha(\mu^2) \log \frac{Q^2}{\mu^2}} \quad (Q^2 \gg \mu^2) \quad (2.2)$$

$$\text{with } b_0 = \frac{11}{3} N_c - \frac{2}{3} N_f \quad (2.3)$$

N_c being the number of colours (=3) and N_f being the number of quark flavours excited at Q^2 . The important point is now that $b_0 > 0$ for $N_f < 16$, i.e., the running coupling $\alpha(Q^2)$ is here decreasing with increasing Q^2 . This behaviour is therefore called "asymptotic freedom". This means that at very small distances quarks behave as almost free particles.

The reason why b_0 is positive is contained in the first term in (2.3) which stems from the gluon loop shown above. The appearance of the gluon loop is a consequence of the gluon self-coupling. There is however no photon self-coupling in QED.

It is convenient to express (2.2) in a little different form. One can see that $\frac{4\pi}{\alpha_s(Q^2)} - b_0 \log Q^2 = \frac{4\pi}{\alpha_s(\mu^2)} - b_0 \log \mu^2 = \text{const.} \equiv -b_0 \log \Lambda^2$.

Here we have introduced the "renormalization invariant" parameter Λ (with the dimension of a mass), thus getting

$$\boxed{\alpha_s(Q^2) = \frac{4\pi}{b_0 \log Q^2/\Lambda^2}} \quad , \quad b_0 = 11 - 2N_f/3 \quad (2.4)$$

$$Q^2 \gg \Lambda^2$$

Λ , the only intrinsic parameter of QCD, has to be determined by experiment ($\Lambda_{\overline{MS}} = 100 \div 400$ MeV in the so called \overline{MS} renormalization scheme). Since the perturbative formula breaks down as $Q^2 \rightarrow \Lambda^2$, i.e. approaching the size of a hadron (where the quarks are supposed to be confined) with ~ 1 fm, we expect $\Lambda \sim 0.2$ GeV

2.3. Applications

The value of eq. (2.4) lies in the possibility of a perturbative treatment of QCD in a range where $\alpha_s(Q^2) \ll 1$, that is at $Q^2 \gg 1 \text{ GeV}^2$, or equivalently in the small distance domain

This is realized in the following processes:

- $e^+e^- \rightarrow X$, $\sqrt{s} \gg 1$ GeV
- deep inelastic lepton-hadron scattering $\ell N \rightarrow \ell' X$
- large p_T processes in hadron-hadron scattering
- production of large mass lepton pairs in hadron-hadron scattering (Drell-Yan process)
- W,Z production in hadron-hadron scattering
- heavy particle production

Perturbative methods are clearly not applicable to the bound-state problem of QCD (i.e. for calculating the hadron masses, etc... or how quarks and gluons finally form colourless hadrons). Although it has not proved possible to demonstrate conclusively that confinement is a consequence of QCD, most physicists believe that QCD is the right theory of strong interactions.

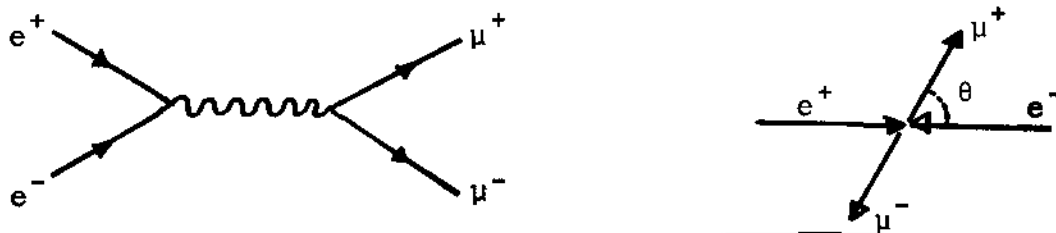
The "soft" hadronic processes, i.e., elastic scattering, diffraction and multiparticle production at small p_T comprise the bulk of scattering data ($> 10^3$ more than high p_T events). Here QCD can not be

applied in a perturbative way, but the whole quark-gluon picture can be used as a sensible guide. Surprisingly (and fortunately) we observe many features in multiparticle production which we can compare with those of "hard" scattering processes.

3. Testing QCD in $e^+e^- \rightarrow \text{hadrons}$

3.1. The simple quark picture

Let us first consider the QED reaction $e^+e^- \rightarrow \mu^+\mu^-$



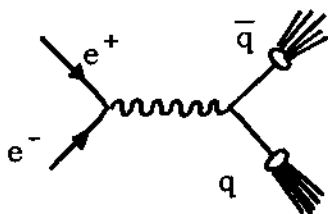
In the lowest order (one photon exchange) approximation the total cross section and the angular dependence is given by ($s \equiv (p_{e^+} + p_{e^-})^2 \gg m_e^2$)

$$\sigma(e^+e^- \rightarrow \mu^+\mu^-) = \frac{4\pi\alpha^2}{3s} e_\mu^2 = \frac{86.6}{s} \text{ nb} \quad (3.1)$$

where $e_\mu = -1$ (the charge of the μ)

$$\frac{d\sigma}{d(\cos\theta)} = \frac{\pi\alpha^2}{2s} e_\mu^2 (1 + \cos^2\theta) \quad (3.2)$$

Within the quark picture we imagine the process $e^+e^- \rightarrow \text{anything}$ as follows



The photon couples directly to a quark and anti-quark (each carrying colour) which then "fragment" into hadrons. (Since quarks fragment into anything with the probability of 1 we do not have to care about this fragmentation process for the moment).

The cross section can therefore be written analogously to eq. 3.1

$$\sigma(e^+e^- \rightarrow q\bar{q})_{s \rightarrow \infty} = \frac{4\pi\alpha^2}{3s} \sum_q e_q^2 \cdot 3$$

and

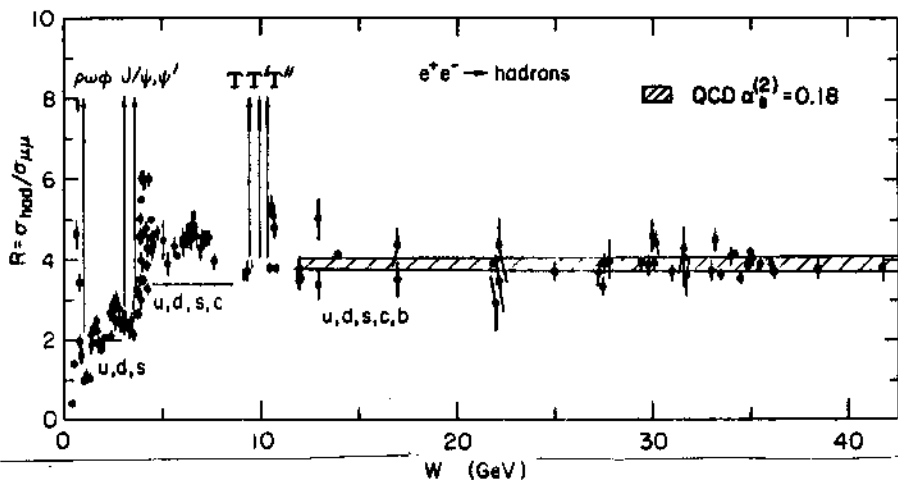
$$R = \frac{\sigma(e^+e^- \rightarrow \text{hadrons})}{\sigma(e^+e^- \rightarrow \mu^+\mu^-)} = 3 \sum_q e_q^2 \quad (3.3)$$

where the sum goes over the quark pairs (which can contribute at the available centre of mass energy). The factor 3 accounts for the 3 colours.

For R we have the following values:

$$\begin{aligned} R &= 2 && u, d, s \\ &= 10/3 && u, d, s, c \\ &= 11/3 && u, d, s, c, b \end{aligned}$$

The behaviour of R as shown in the following figure ($W = \sqrt{s}$)



is indeed one of the most beautiful confirmations of this picture

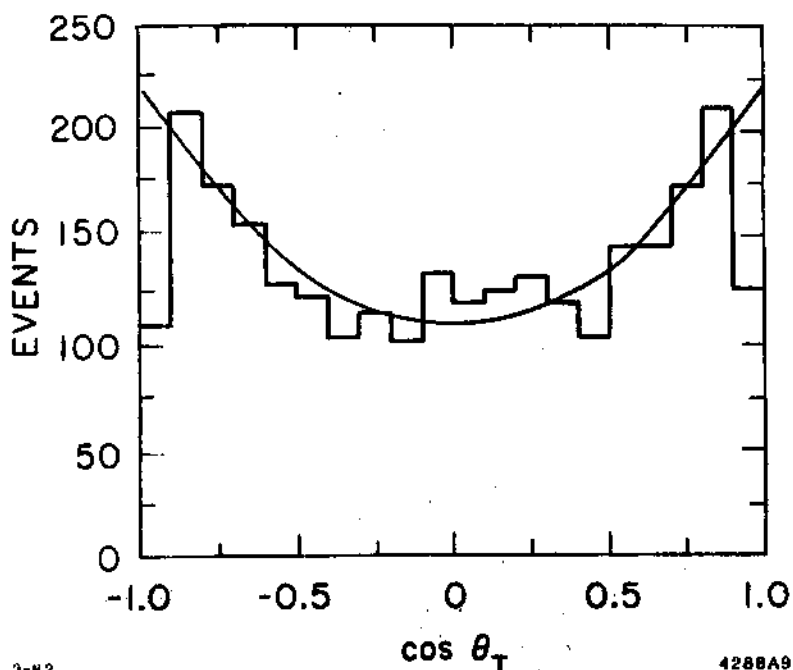
-15-

and shows that the colour degree of freedom is really needed to explain the data.

At high energies quarks should be seen as hadron jets. They are clearly seen in experiment for $\sqrt{s} > 7$ GeV.

If quarks have spin 1/2 the angular distribution of a quark (jet) should go as $\sim (1 + \cos^2\theta)$ according to eq. 3.2.

The data



show this behaviour (θ_T is the angle of the thrust axis (\approx quark axis, see below)).

A further consequence of the point-like nature of quarks is that the break-up of the quark into hadrons to form a jet should be independent of s . Thus we expect the cross section to scale.

$$\frac{d\sigma}{dz} \sim \frac{1}{s} D(z) \quad \text{where } z = \frac{2E_h}{\sqrt{s}} \quad (3.4)$$

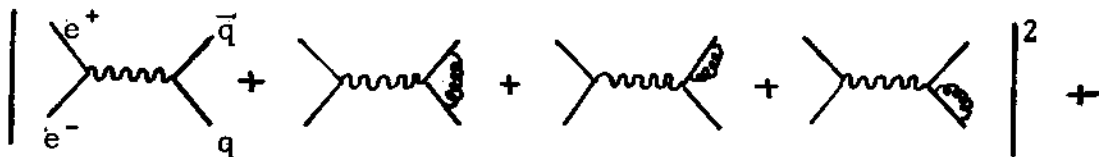
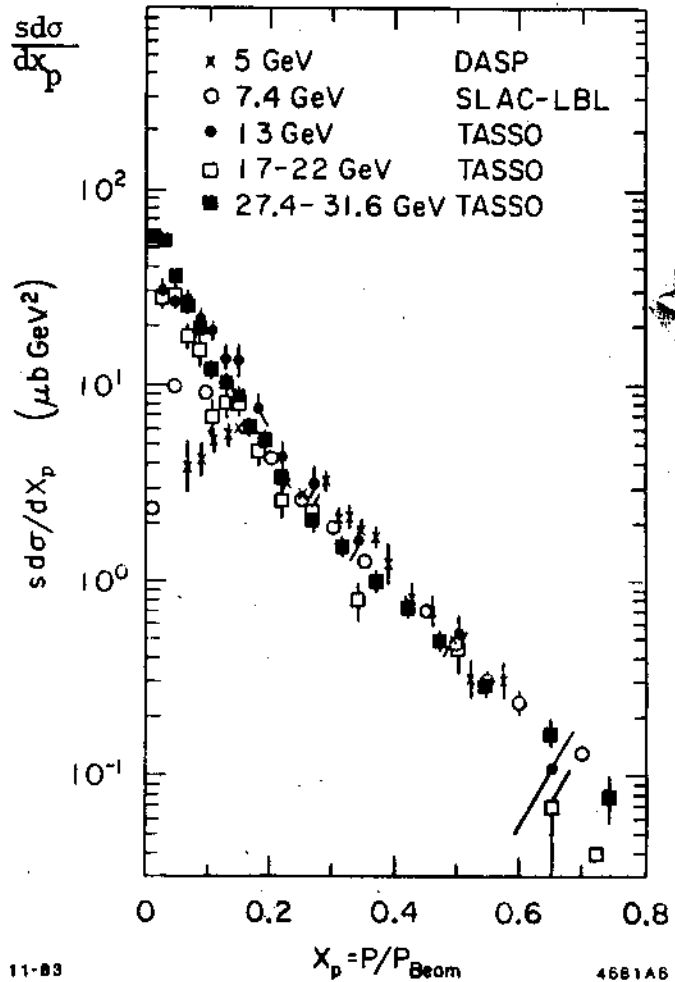
(E_h is the hadron energy). Although small violations are seen

(+ QCD corrections) this scaling works quite well (at least for $z > 0.2$). (See Figure, here $z=x_p$.)

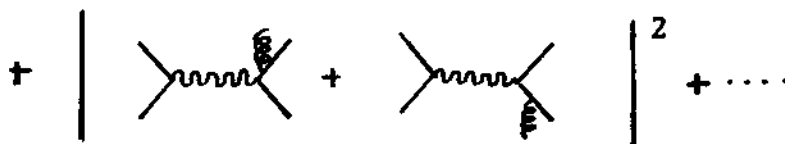
4. Effects of QCD - $O(\alpha_s)$ corrections, 3 jet events

4.1 - The total cross section

In QCD we expect quarks to radiate gluons and therefore the following processes to contribute to the cross section $e^+e^- \rightarrow \text{hadrons}$:



(A)



(B)

In graphs (A) the gluon is virtual whereas in (B) it is real.

(The absolute sum squared has of course to be taken where the

final state is indistinguishable). It is interesting to note that

the diagrams (B) exhibit an "infrared" divergence either if the gluon energy is zero or if the gluon goes into the same direction as the quark or antiquark (due to the zero mass of the gluon and the quark). However, in the total sum (A)+(B) of virtual and real gluon contributions the divergences cancel !

We thus get the result

$$R = 3 \sum_q e_q^2 \left[1 + \frac{\alpha_s(s)}{\pi} \left(1 + c \frac{\alpha_s}{\pi} \right) + \dots \right] \quad (4.1)$$

(with $c = 0.08$ in the \overline{MS} scheme).

This is considered one of the "cleanest" predictions of QCD.

Unfortunately R measurements are very difficult. The average over results obtained by JADE, MARK J, TASSO, MAC, MARK II at $\langle s \rangle = 1170 \text{ GeV}^2$ is

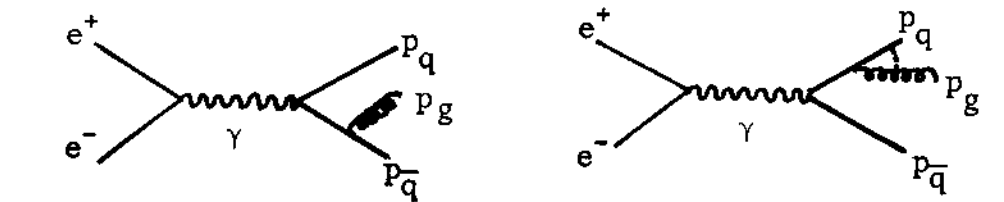
$$\langle \alpha_s \rangle = 0.190 \pm 0.015 \pm 0.047$$

(stat.) (syst.)

So far for the inclusive cross section. But wouldn't it be a clearer test of the existence of gluons if we could see gluon jets ?

4.2. The gluon jet: $e^+e^- \rightarrow q\bar{q}g$

For studying $e^+e^- \rightarrow q\bar{q}g$ events which yield 3 jets in the final state we have to consider the following diagrams



Define $\hat{s} = (p_\gamma - p_q)^2 = s(1-x_q)$
 $\hat{t} = (p_\gamma - p_{\bar{q}})^2 = s(1-x_{\bar{q}})$ (neglecting masses)
 $\hat{u} = (p_\gamma - p_g)^2 = s(1-x_g)$

where we have introduced $x_q = E_q/\sqrt{s}/2$, $x_{\bar{q}} = E_{\bar{q}}/\sqrt{s}/2$, $x_g = E_g/\sqrt{s}/2$ fulfilling the relation

$$x_q + x_{\bar{q}} + x_g = 2.$$

Calculating the graphs above leads to the (matrix element)²:

$$|M|^2 \propto \left(\frac{\hat{t}}{\hat{s}} + \frac{\hat{s}}{\hat{t}} + \frac{2\hat{u}\hat{s}}{\hat{s}\hat{t}} \right) = \frac{x_q^2 + x_{\bar{q}}^2}{(1-x_q)(1-x_{\bar{q}})}$$

(the poles at $\hat{s}, \hat{t} = 0$ coming from the quark propagator).

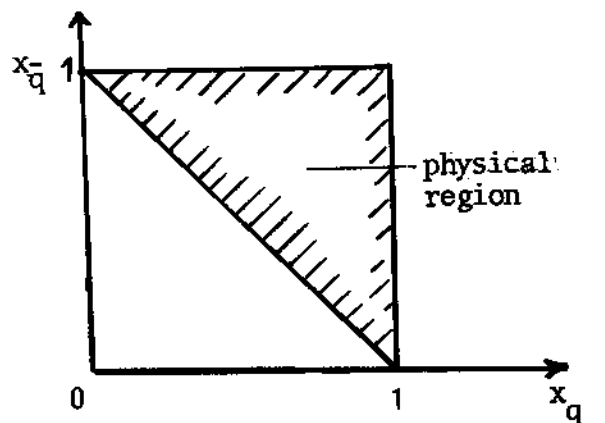
The cross section for $e^+e^- \rightarrow q\bar{q}g$ then reads:

$$\boxed{\frac{1}{\sigma} \frac{d\sigma}{dx_q dx_{\bar{q}}} = \frac{2\alpha_s}{3\pi} \frac{x_q^2 + x_{\bar{q}}^2}{(1-x_q)(1-x_{\bar{q}})}} \quad (4.2)$$

Here $\sigma = \sigma(e^+e^- \rightarrow q\bar{q}) = \frac{4\pi\alpha^2}{s} e_q^2$ (the two jet cross sections).

The kinematically allowed region of x_q and $x_{\bar{q}}$ is the triangle

Since $\hat{t} = s(1-x_{\bar{q}}) = (p_q + p_g)^2 = 2E_q E_g (1-\cos\theta)$ we again meet a singularity either if $E_g \rightarrow 0$ or the gluon and the quark are collinear (see 4.1). In an experiment appropriate cuts are made to separate off the



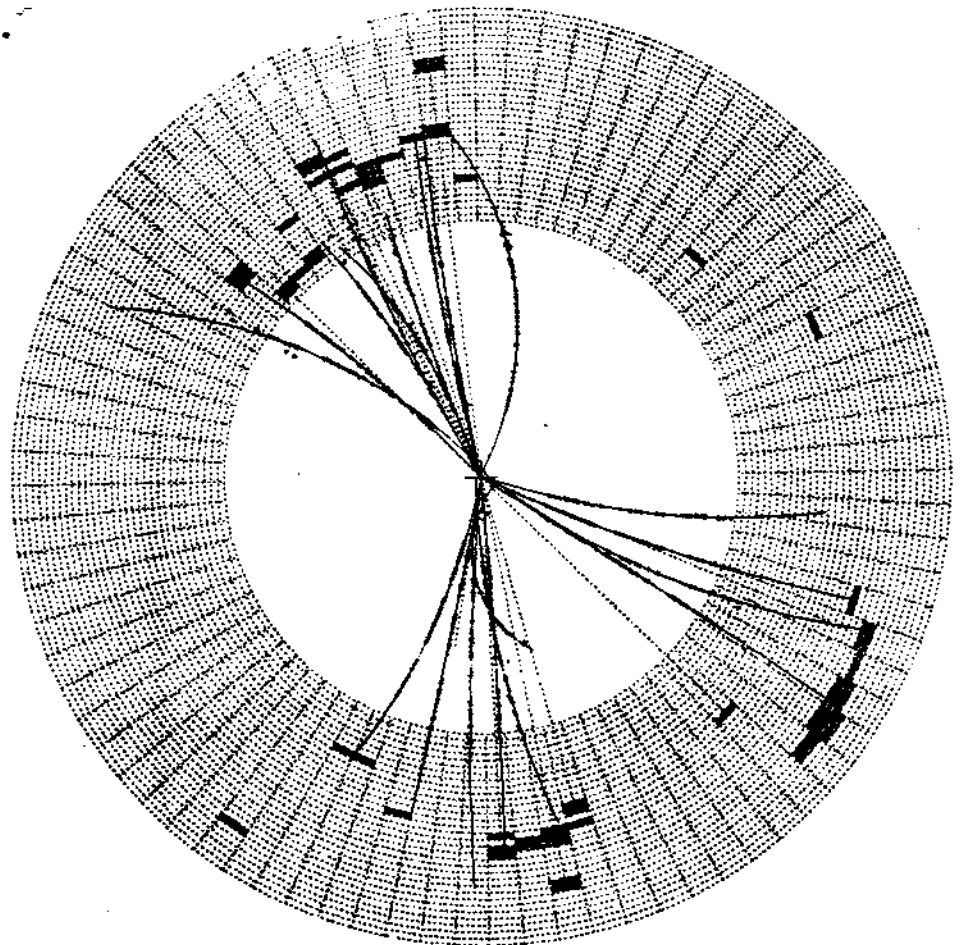
three jet events. We already saw in

4.1 that in the totally inclusive cross section these divergences cancel.

If E_g and θ are not too small, we can expect to see a third (gluon) jet in addition to the two quark jets. One would expect

$$\frac{\sigma_{3 \text{ jet}}}{\sigma_{2 \text{ jet}}} \sim \alpha_s$$

that is, only $\sim 10\%$ of all events will show a 3 jet structure (at present energies).



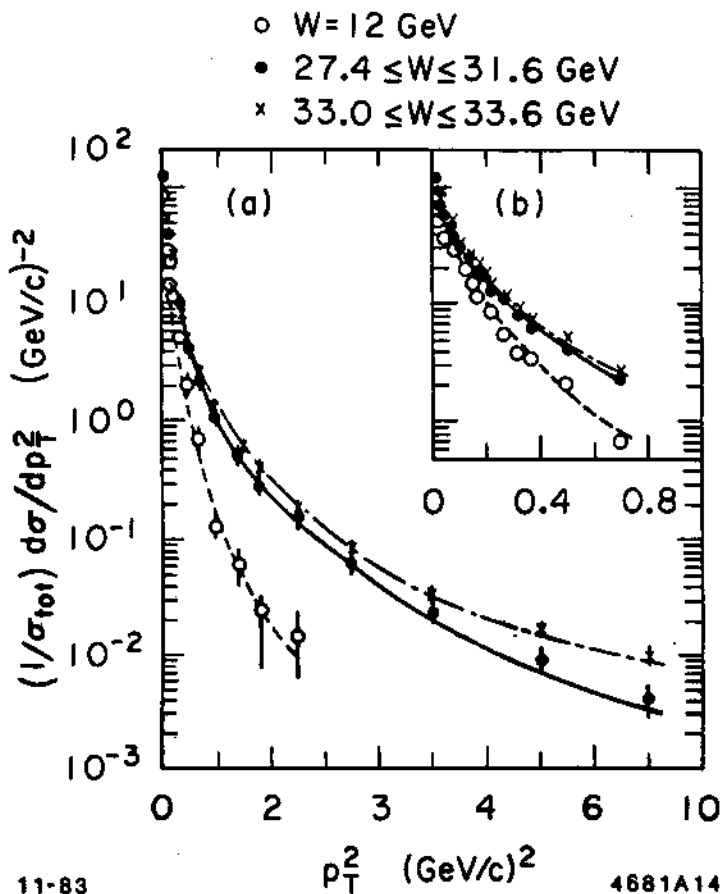
A three-jet event observed by the JADE detector at PETRA.

In most cases we have therefore two jets. For small E_g and θ the quark (antiquark) gets a transverse momentum p_T with respect to $\bar{q}(q)$ by radiating off a gluon. According to eq. 4.2

$$\frac{d\sigma}{dp_T} \propto \frac{\alpha_s}{p_T} \quad (\text{with } \alpha_s \sim \frac{1}{\ln s})$$

and therefore $\langle p_T \rangle \sim \int^{\sqrt{s}} p_T \frac{d\sigma}{dp_T} \propto \alpha_s \sqrt{s}$

We see a clear increase in $\langle p_T \rangle$ in the data ($W = \sqrt{s}$):



Transverse momentum distribution of hadrons relative to the thrust (=jet) axis for different e^+e^- centre of mass energies.

The hadrons have even in a pure two quark jet event a $\langle p_T \rangle \approx 300$ MeV. It can be shown that the increase with \sqrt{s} is mainly in the event plane, that is, due to the appearance of planar qqq events.

4.3. Jet measures

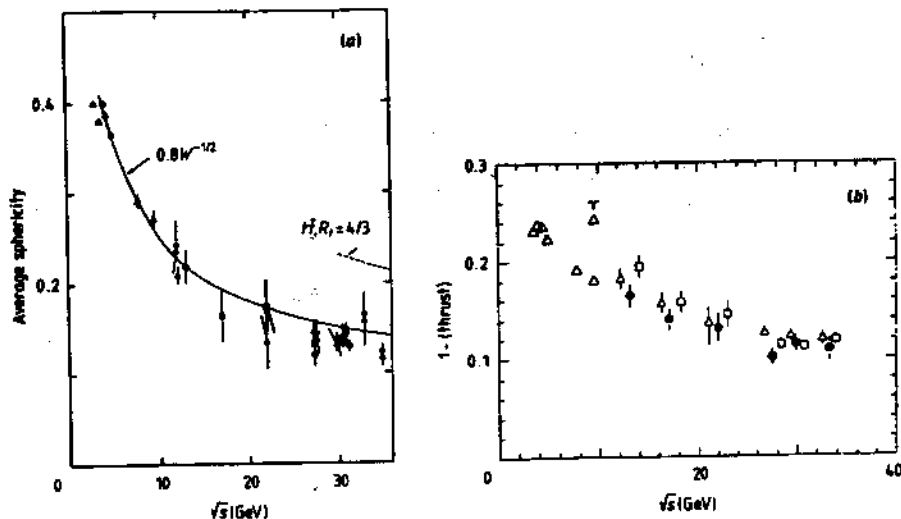
The most known measures of the degree of "jettiness" are

$$\text{sphericity} \quad S \equiv \min \left(\frac{3}{2} \frac{\sum_i p_{T_i}^2}{\sum_i p_i^2} \right)$$

and

$$\text{thrust} \quad T \equiv \max \left(\frac{\sum_i |p_{L_i}|}{\sum_i p_i} \right)$$

That is, one looks for the axis such that the sum of transverse momenta p_{T_i} over all particles is a minimum or the sum of their longitudinal momenta is a maximum. If there were no jets and all momentum directions are equally probable, then $S = 1$ or $T = 1/2$. Pure jets give $S \rightarrow 0$ and $T \rightarrow 1$. We expect $\langle S \rangle$ and $1 - \langle T \rangle$ to decrease with energy



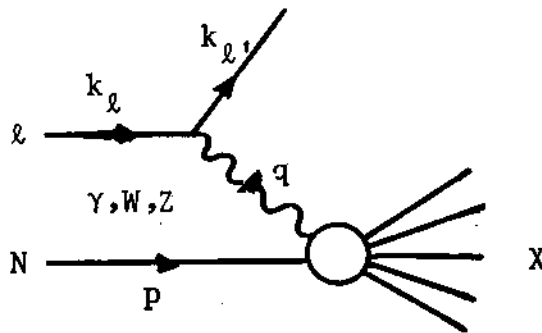
The average sphericity (a) and $1 - \text{thrust}$ (b) as a function of the e^+e^- CM energy (Wolf 1980).
 X JADE, Δ PLUTO, \bullet TASSO, \square MARK-J.

5. Deep inelastic lepton-hadron scattering

Historically the deep inelastic (= high momentum transfer) scattering of electrons on a nucleon was the starting point of the modern quark-parton picture which subsequently led to the development of QCD. From studying these processes we also learned most about the structure of the nucleon.

5.1. Kinematics

We shall consider the reaction $\ell + N \rightarrow \ell' + X$



i.e.

- | | | |
|---------------------------------------|---------------------------------------|---------------------------|
| $e^- N \rightarrow e^- X$ | electroproduction | } (exchange of γ) |
| $\mu^- N \rightarrow \mu^- X$ | muon production | |
| $\nu N \rightarrow \mu^- X$ | } charged current neutrino scattering | (exchange of W^\pm) |
| $\bar{\nu} N \rightarrow \mu^+ X$ | | |
| $(-)\nu N \rightarrow (-)\bar{\nu} X$ | neutral current neutrino scattering | (exchange of Z) |

Usually the following kinematic variables are defined:

$$q = k_{\ell'} - k_{\ell},$$

$$Q^2 = -q^2 = 4E_{\ell}E_{\ell'} \sin^2 \theta/2$$

$$\nu = \frac{pq}{M} = E_{\ell} - E_{\ell'} = E_X$$

(in the lab system)

where M is the nucleon mass.

$$W \text{ (inv. mass of hadronic system } X) = \sqrt{M^2 - Q^2 + 2M\nu}$$

The kinematic region is given by

$$0 \leq W^2 = -Q^2 + M^2 + 2\nu M$$

and hence

$$Q^2 \leq 2\nu M + M^2$$

Instead of ν, Q^2 often the dimensionless Bjorken scaling variables are used

$$\boxed{\begin{aligned} x &\equiv \frac{Q^2}{2M\nu} = \frac{2E_\ell E_{\ell'} \sin^2 \theta/2}{ME_x} \\ y &\equiv \frac{\nu}{E_\ell} = \frac{pq}{pk_\ell} = \frac{E_x}{E_\ell} \end{aligned}} \quad \begin{aligned} 0 \leq x \leq 1 \\ 0 \leq y \leq 1 \end{aligned} \quad (5.1)$$

Electro- or Muon production

It can be quite generally described by two structure functions $W_1(\nu, Q^2)$ and $W_2(\nu, Q^2)$

$$\frac{d^2\sigma(eN+eX)}{dQ^2 d\nu} = \frac{4\pi\alpha^2}{q^4} M \frac{E_{\ell'}}{E_\ell} [W_2(\nu, Q^2) \cos^2 \theta/2 + 2W_1(\nu, Q^2) \sin^2 \theta/2]$$

where W_1 and W_2 are related to the transverse and longitudinal cross section.

Defining $F_1(x, Q^2) = W_1(\nu, Q^2)$

$$F_2(x, Q^2) = \frac{\nu W_2(\nu, Q^2)}{M}$$

we can write it also in the form

$$\frac{d^2\sigma(eN \rightarrow eX)}{dx dy} = \frac{4\pi\alpha^2}{Q^4} s [F_2(x, Q^2)(1-y) + xF_1(x, Q^2)y^2]$$

$$(s = (k_\ell + p)^2 = 2E_\ell M)$$

(5.2)

Neutrino scattering

Here we have three structure function $F_1(x, Q^2)$, $F_2(x, Q^2)$ and $F_3(x, Q^2)$, the latter of which is a parity violating term not present in electroproduction.

The cross section reads (for $Q^2 \ll M_W^2$, M_W being the W mass)

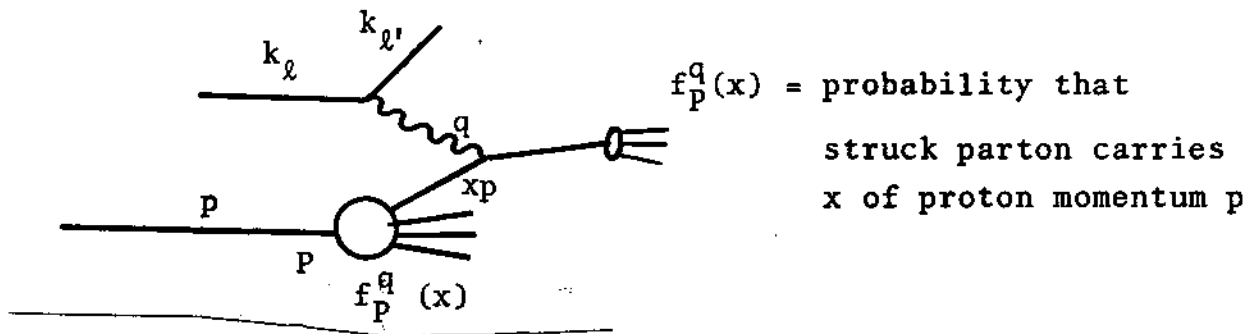
$$\frac{d^2\sigma(\nu N + \mu^- X)}{dx dy} = \frac{G^2 M E_\nu}{\pi} \{ xy^2 F_1^{\nu, \bar{\nu}}(x, Q^2) + (1-y) F_2^{\nu, \bar{\nu}}(x, Q^2) \pm xy (1 - \frac{1}{2}y) F_3^{\nu, \bar{\nu}}(x, Q^2) \}$$

(with $G \approx 10^{-5} M^{-2}$)

(5.3)

5.2. Quark-parton model

If Q^2 is large, i.e. at small distances, we can imagine the nucleon consisting of almost free point-like particles (partons). These partons are identified with the 3 valence quarks and a "sea" of $q\bar{q}$ pairs. As we shall see, there are in addition also gluons present (to which, of course, the photon, W or Z does not couple directly). The scattering can therefore be visualized as follows:



i.e., we have actually a lepton scattering off point-like partons contained in the proton. We thus can write:

$$\frac{d^2\sigma(\ell P \rightarrow \ell' X)}{dx dy} = \sum_q f_P^q(x) \frac{d\sigma}{dx dy}(\ell q \rightarrow \ell' q') \quad (5.4)$$

This is the master equation for lepton-hadron scattering within the quark-parton picture. Here x as defined above coincides with the Bjorken x as given in eq. (5.1) as can be seen:

$m^2 \approx 0 = (q+px)^2 \approx q^2 + 2xqp$. This means that a given Q^2 and v determine the x value of the quark from which the electron has scattered. We call $f_P^q(x)$ the quark distribution functions.

5.2.1. Electron scattering

Let us, for simplicity, discuss first electron-scattering. It is straightforward to calculate $eq \rightarrow eq$. Eq. (5.4) then reads:

$$\left(\frac{d^2}{dx dy}\right)_{eP \rightarrow eX} = \frac{2\pi\alpha^2}{Q^4} s [1+(1-y)^2] \sum_q e_q^2 x f_P^q(x) \quad (5.5)$$

By comparing it with the general formula eq. (5.2) we observe the following:

$$F_2(x) = \sum_q e_q^2 x f_P^q(x) \quad (5.6)$$

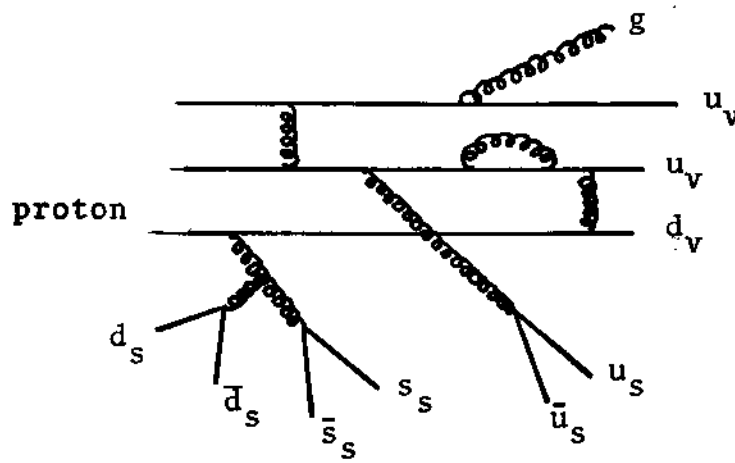
$$2xF_1(x) = F_2(x) \quad (\text{Callan - Gross relation})$$

$$F_1(x), F_2(x) \text{ being only dependent on } x \\ \rightarrow \text{Bjorken scaling}$$

It should be remembered here that it was the observation of (approximate) scaling in deep inelastic scattering which provided the principal motivation for introducing the quark-parton model. The Callan-Gross relation is simply a consequence of spin 1/2 quarks. (It is satisfied up to terms of order α_s).

Quark distributions

We can imagine a proton as in the following figure



The distribution functions $f_P^q(x)$ of quarks inside a proton are called $u(x)$, $d(x)$, $s(x)$, $\bar{u}(x)$, $\bar{d}(x)$, $\bar{s}(x)$ (neglecting the heavier quarks).

For $eP \rightarrow eX$ we then have from eq. (5.6):

$$\begin{aligned} \frac{1}{x} F_2^{eP}(x) &= \left(\frac{2}{3}\right)^2 [u(x) + \bar{u}(x)] + \left(\frac{1}{3}\right)^2 [d(x) + \bar{d}(x)] \\ &+ \left(\frac{1}{3}\right)^2 [s(x) + \bar{s}(x)] \end{aligned}$$

and by charge symmetry for $en \rightarrow eX$ (n - neutron) we just have to replace $u \longleftrightarrow d$:

$$\begin{aligned} \frac{1}{x} F_2^{en}(x) &= \left(\frac{2}{3}\right)^2 [d(x) + \bar{d}(x)] + \left(\frac{1}{3}\right)^2 [u(x) + \bar{u}(x)] \\ &+ \left(\frac{1}{3}\right)^2 [s(x) + \bar{s}(x)] \end{aligned}$$

The $u(x)$ and the $d(x)$ can be decomposed into a valence and a "sea" quark parton:

$$\begin{array}{|l} u(x) = u_V(x) + u_S(x) \\ d(x) = d_V(x) + d_S(x) \end{array} \quad (5.7)$$

whereas for the "sea" ($u_S \bar{u}_S, d_S \bar{d}_S, \bar{s}_S s_S, \dots$) we assume SU(3) flavour symmetry thus having

$$u_S(x) = \bar{u}_S(x) = d_S(x) = \bar{d}_S(x) = s_S(x) = \bar{s}_S(x) \equiv S(x)$$

sea distribution

Sum rules

The distribution functions have to fulfill sum rules since, for instance, the number of valence u quarks in the proton has to be 2

$$\int_0^1 [u(x) - \bar{u}(x)] dx = 2$$

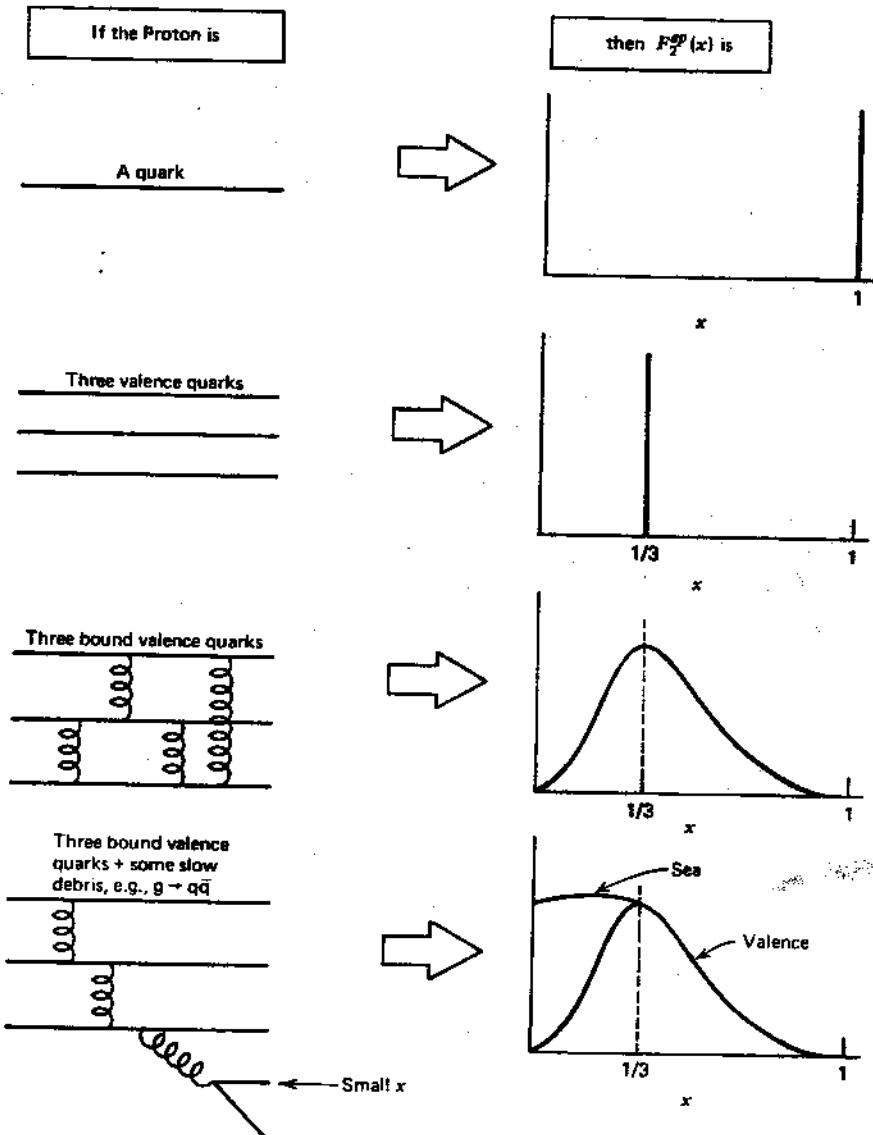
and analogously

$$\int_0^1 (d - \bar{d}) dx = 1$$

$$\int_0^1 (s - \bar{s}) dx = 0$$

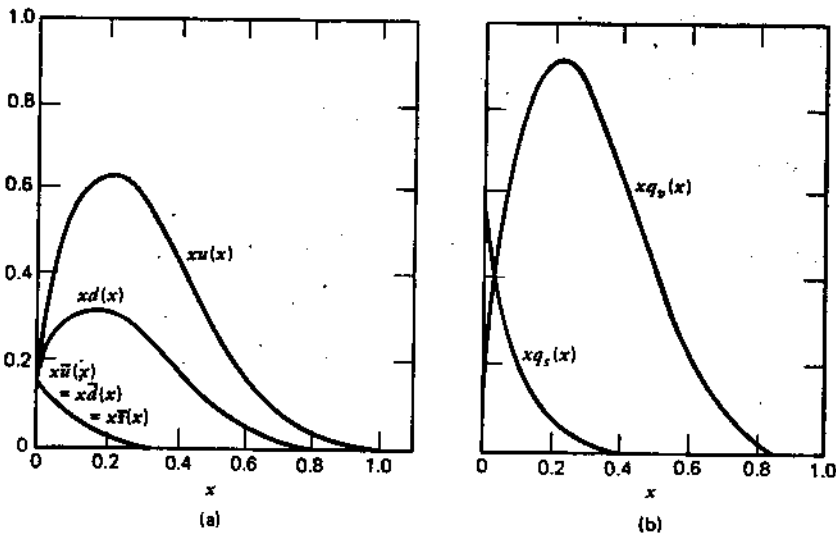
Which behaviour would we expect for $F_2(x)$?

The following picture should illustrate it:



The structure function pictured corresponding to different compositions assumed for the proton.

This was indeed seen in the data. The following figure exhibits the quark distribution as extracted from deep inelastic scattering data (including neutrino scattering data).



The quark structure functions extracted from an analysis of deep inelastic scattering data. Figure (b) shows the total valence and sea quark contributions to the structure of the proton.

We see that the sea is negligible for $x \geq 0.3$.

- But where are the gluons ?

Let us consider the momentum (conservation) sum rule following from the definition of $f_p^q(x)$:

$$\sum_q \int_0^1 (px) f_p^q(x) dx = p \rightarrow \int_0^1 dx \cdot x (u + \bar{u} + d + \bar{d} + s + \bar{s}) \stackrel{?}{=} 1$$

Putting in the experimental structure functions on the left hand side we only get 0.54 instead of 1. This means that 46% of the total momentum of the nucleon is carried by electrically neutral constituents, the gluons.

-What do we expect for the x-dependence of quark distributions ?

Assuming Regge behaviour for the process $\gamma^* + N \rightarrow X$, that is by identifying the sea-quark distribution with Pomeron exchange

($\alpha_p(0) \approx 1$) and the valence part with the leading particle exchange

($f, A_2, \dots; \alpha_R(0) \sim \frac{1}{2}$) one gets for $x \rightarrow 0$

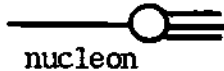
$$\text{sea} \xrightarrow{x \rightarrow 0} 1/x$$

$$\text{valence quarks} \xrightarrow{x \rightarrow 0} 1/\sqrt{x}$$

For $x \rightarrow 1$, there have been invented various counting rules. We just mention one of them

$$f_n^q(x) \underset{x \rightarrow 1}{\sim} (1-x)^{2n-3}$$

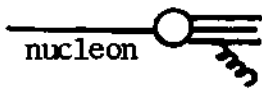
where n is the number of constituents. Examples are



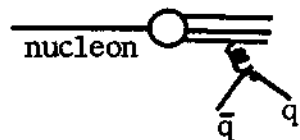
$$u_v, d_v \underset{x \rightarrow 1}{\sim} (1-x)^{2 \cdot 3 - 3} = (1-x)^3$$



$$(1-x)^1$$



$$g \underset{x \rightarrow 1}{\sim} (1-x)^{2 \cdot 4 - 3} = (1-x)^5$$



$$\text{sea} \underset{x \rightarrow 1}{\sim} (1-x)^{2 \cdot 5 - 3} = (1-x)^7$$

We thus have the behaviour (which however works only very approximately)

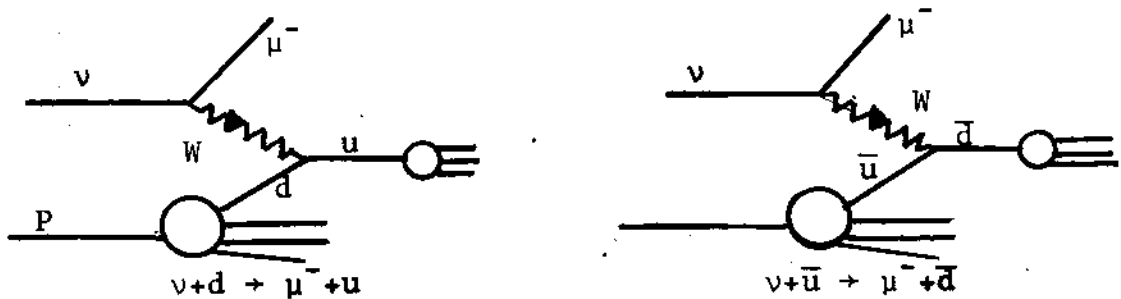
$$f_n^{(q)}(x) \sim x^{-\alpha} (1-x)^{2n-3} \quad \text{where } \alpha(0) = 1 \quad \text{and } = 1/2$$

for the sea and valence part, respectively.

5.2.2 Neutrino scattering

The simple quark parton picture:

The general formula was given in eq. (5.3). In the simple quark parton picture the process is again the result of a point-like interaction with the quarks inside the proton



We just calculate the subprocesses $\nu+d \rightarrow \mu^-+u$ and $\nu+\bar{u} \rightarrow \mu^-+\bar{d}$. By using the corresponding master formula eq. (5.4) we obtain:

$$\frac{d^2\sigma(\nu P \rightarrow \mu^- X)}{dx dy} = \frac{2G^2 M E_\nu x}{\pi} [d(x) + \bar{u}(x)(1-y)^2] \quad (5.8)$$

Here we put the Cabibbo angle $\cos^2\theta_c = 1$ and neglected s, c, \dots quarks for simplicity.

For $\bar{\nu}P$ scattering we have to consider $\bar{\nu}u \rightarrow \mu^+d$ and $\bar{\nu}\bar{d} \rightarrow \mu^+\bar{u}$ thus arriving at (with $\sigma_0 = 2G^2 M E_\nu / \pi$)

$$\frac{d^2\sigma(\bar{\nu}P \rightarrow \mu^+ X)}{dx dy} = \sigma_0 x [\bar{d}(x) + u(x)(1-y)^2] \quad (5.9)$$

For scattering off an isoscalar target, where most experiments have

been done, one defines:

$$q(x) \equiv x[u(x) + d(x) + s(x) + c(x)]$$

$$\bar{q}(x) = x[\bar{u}(x) + \bar{d}(x) + \bar{s}(x) + \bar{c}(x)]$$

getting

$$\frac{d\sigma^{\nu N}}{dx dy} = \sigma_0 [q(x) + \bar{q}(x)(1-y)^2]$$

$$\frac{d\sigma^{\bar{\nu} N}}{dx dy} = \sigma_0 [\bar{q}(x) + q(x)(1-y)^2]$$

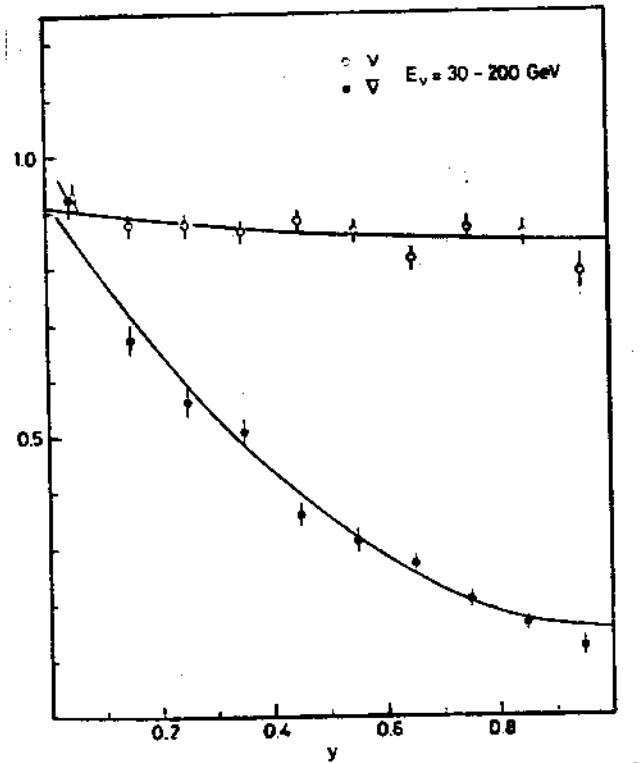
- From these expressions due to the suppressed sea contribution one expects for ν -scattering a rather flat y -dependence and a dependence $\sim (1-y)^2$ for $\bar{\nu}$ -scattering:

- From the simple quark-parton model again a scaling behaviour of x follows, which is approximately realised in experiment.

- From the ratio of neutrino to antineutrino scattering $\sigma^{\bar{\nu}}/\sigma^{\nu}$ we can find the ratio of the momenta carried by antiquarks and quarks within the nucleon:

$$\frac{\langle \bar{q} \rangle}{\langle q \rangle} = \frac{\sigma^{\bar{\nu}}/\sigma^{\nu} - 1/3}{1 - \frac{1}{3} \sigma^{\bar{\nu}}/\sigma^{\nu}} \approx 0.18$$

with $(\sigma^{\bar{\nu}}/\sigma^{\nu})_{\text{exp.}} = 0.48$. (From eq. (5.8) we see that the total



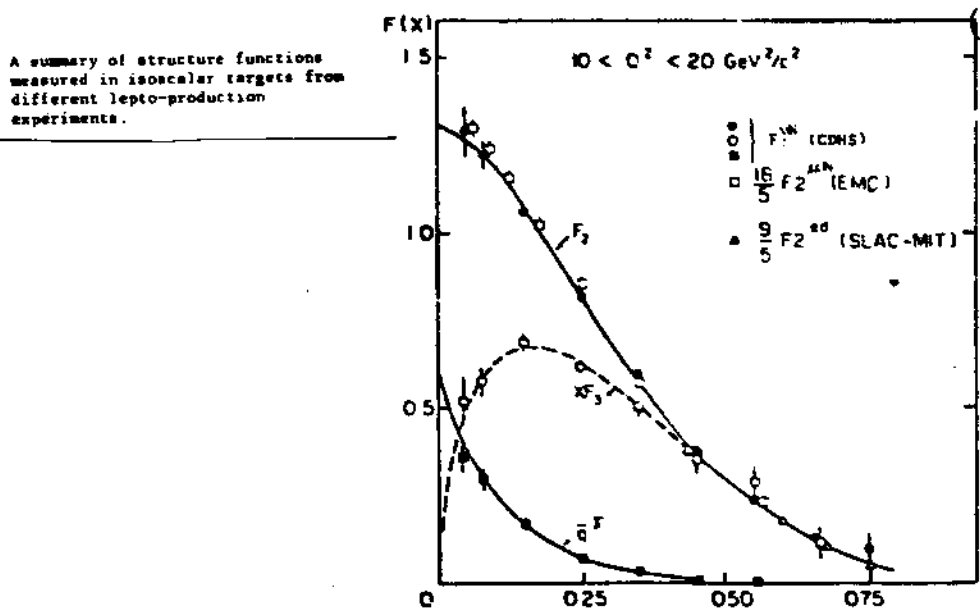
ν and $\bar{\nu}$ cross sections rise linearly with the neutrino energy E_ν).
 - With the functions F_2, F_3 as defined in the general expressions eq. (5.3) we have the following relations important for comparisons with experiment:

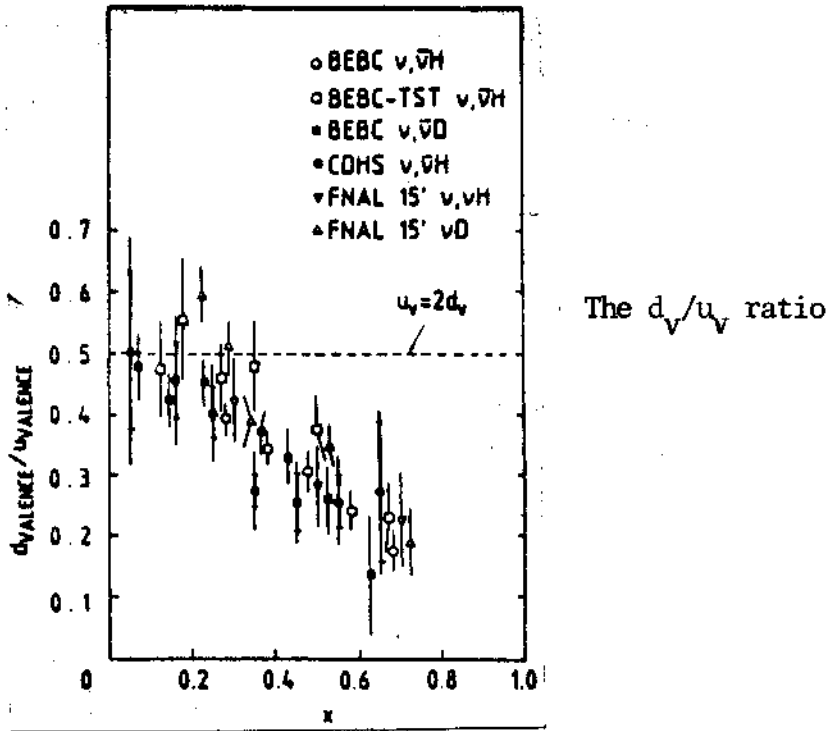
$$xF_3(x, Q^2) = \frac{\pi}{G^2 M^2 E_\nu} \frac{\sigma(\nu N) - \sigma(\bar{\nu} N)}{1 - (1-y)^2} = q(x, Q^2) - \bar{q}(x, Q^2)$$

(pure valence quark distributions)

$$F_2(x, Q^2) = \frac{\pi}{G^2 M^2 E_\nu} \frac{\sigma(\nu N) + \sigma(\bar{\nu} N)}{1 + (1-y)^2 - y^2 R'} = q(x, Q^2) + \bar{q}(x, Q^2)$$

where $R' \equiv 1 - \frac{2xF_1}{F_2} = 0$ in the simple quark parton picture (Callan-Gross relation, see section 5.2.1) and small experimentally. We already put F_i and q as function of x and Q^2 because - as we shall see - they also have a weak Q^2 dependence due to QCD-effects. The following figure shows what the F_2, F_3 and \bar{q} distributions look like:

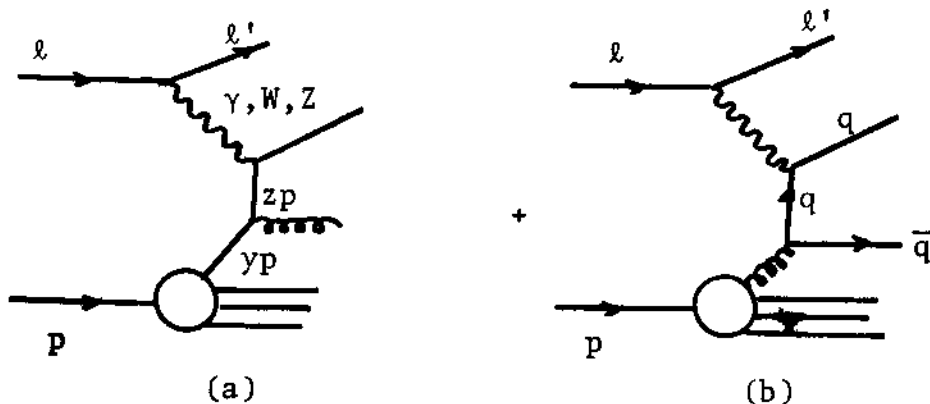




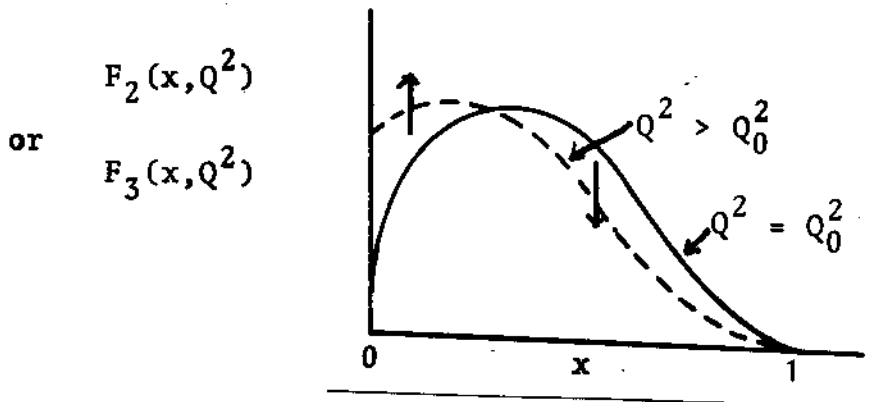
The data also revealed that the d_V distribution is softer than the u_V distribution. The ratio d_V/u_V decreases linearly from ~ 0.6 at $x = 0$ to zero at $x = 1$.

5.3. Influence of gluons (QCD effects)

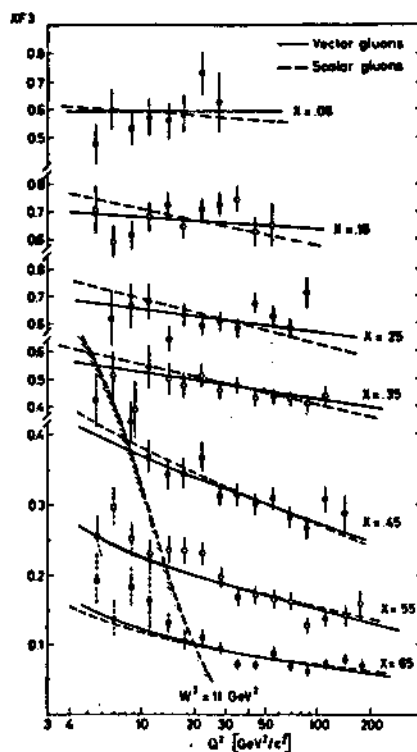
We know that gluons are present in the nucleon and that quarks can radiate off gluons. We therefore have to consider the following diagrams in addition to the ones in section 5.2.



It is easy to see their effect: The photon (W or Z) now "sees" the quark with lower momentum either because it lost some by the radiation of a gluon or because it comes from a gluon splitting into a $q\bar{q}$. The effect is shown in the following picture

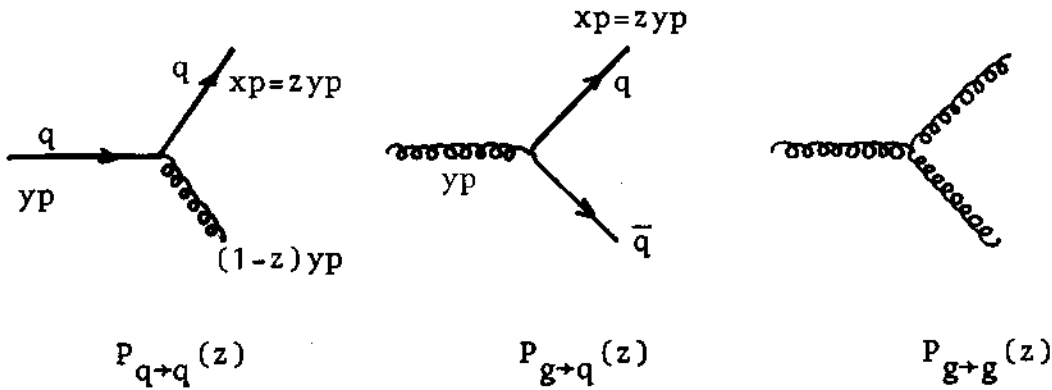


Compare this with the data:



Scaling violations of $x F_3$, measured by CDHS.

QCD is however able to reproduce this behaviour quantitatively. Let us consider the following basic transitions:



The first graphs shows a quark with momentum yp (p being the momentum of the nucleon) emitting a gluon and leaving itself with momentum xp ($x \leq y \leq 1$).

The probability for this to happen is (to first order in α_s)

$$\frac{\alpha_s(Q^2)}{2\pi} P_{q \rightarrow q}\left(\frac{x}{y}\right) \log \frac{Q^2}{Q_0^2} \quad \text{with } z = \frac{x}{y} \quad (\text{scaling})$$

The origin of the log-factor is quite clear. It is due to bremsstrahlung of gluons. Recall our discussion in e^+e^- in section 4.2:

$$\int_{Q_0^2}^{Q^2} \frac{dP_T^2}{P_T^2} \cong \log \left(\frac{Q^2}{Q_0^2} \right)$$

The splitting function $P_{q \rightarrow q}(z)$ is easily calculated from Feynman rules to be

$$P_{q \rightarrow q}(z) = \frac{4}{3} \frac{(1+z^2)}{(1-z)}$$

(The divergence as $z \rightarrow 1$ is cancelled when virtual gluon contributions are included).

We therefore have

The diagram shows five terms representing the structure function $q(x)$ and its corrections. The first term is the tree-level diagram: a vertical line from the bottom left to the top left, a horizontal line from the top left to the top right, and a vertical line from the top right to the bottom right. A wavy gluon line is attached to the top horizontal line. The second term is a tree-level diagram with a gluon line attached to the bottom vertical line. The third term is a tree-level diagram with a gluon line attached to the bottom vertical line and another gluon line attached to the top horizontal line. The fourth term is a one-loop diagram (box diagram) with a gluon line on the left vertical line and another gluon line on the top horizontal line. The fifth term is a one-loop diagram (triangle diagram) with a gluon line on the left vertical line and another gluon line on the top horizontal line.

$$= \underbrace{\int_x^1 \frac{dy}{y} q(y) \left\{ \delta\left(1 - \frac{x}{y}\right) + \frac{\alpha_s(Q^2)}{2\pi} P_{q+q}(x/y) \log \frac{Q^2}{Q_0^2} + \dots P_{g+q}(x/y) \right\}}_{q(x)}$$

One wants to incorporate the leading α_s -corrections into the structure function. One therefore redefines

$$q(x) \rightarrow q(x, Q^2) = q(x) + \frac{\alpha_s}{2\pi} \log\left(\frac{Q^2}{Q_0^2}\right) \int_x^1 \frac{dy}{y} [q(y) P_{q+q}(x/y) + g(y) P_{g+q}(x/y)] + \dots$$

or (to leading order)

$$\frac{dq(x, Q^2)}{d \log Q^2} = \frac{\alpha_s}{2\pi} \int_x^1 \frac{dy}{y} [q(y, Q^2) P_{q+q}(x/y) + P_{g+q}(x/y) g(y, Q^2)]$$

(5.10)

Similarly

$$\frac{dg(x, Q^2)}{d \log Q^2} = \frac{\alpha_s}{2\pi} \int_x^1 \frac{dy}{y} \left[\sum_q P_{q+g}(x/y) q(y, Q^2) + P_{g+g}(x/y) g(y, Q^2) \right]$$

(5.11)

These are the so-called Q^2 -evolution equations by Altarelli-Parisi. $g(x, Q^2)$ is the gluon distribution in analogy to the quark distribution $q(x, Q^2)$.

Although we do not know the structure functions $q(x, Q^2)$ and $g(x, Q^2)$ from first principles the equations above tell us that, once we have measured them at $Q^2 = Q_0^2$, we know how they will change with Q^2 . This is the essence of QCD in deep inelastic scattering.

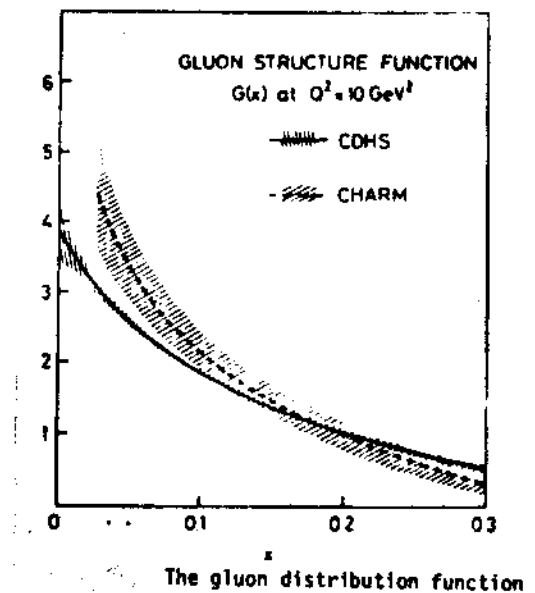
The Altarelli-Parisi equation is particularly simple for $x F_3(x, Q^2)$ where the sea contribution drops out;

$$\frac{d}{d \log Q^2} (x F_3(x, Q^2)) = \frac{\alpha_s(Q^2)}{2\pi} \int_x^1 P_{q \rightarrow q}(x/y) y F_3(y, Q^2) \frac{xdy}{y^2}$$

The left hand side is directly measured (by determining the slopes of $x F_3$). The integral on the right hand side is a convolution of $x F_3$, which is measured up to $x=0,65$. One was thus able to deduce the Λ parameter in the running coupling constant, eq. (2.4):

$$\Lambda_{\overline{MS}} = 0,25 \pm 0,15 \text{ GeV}$$

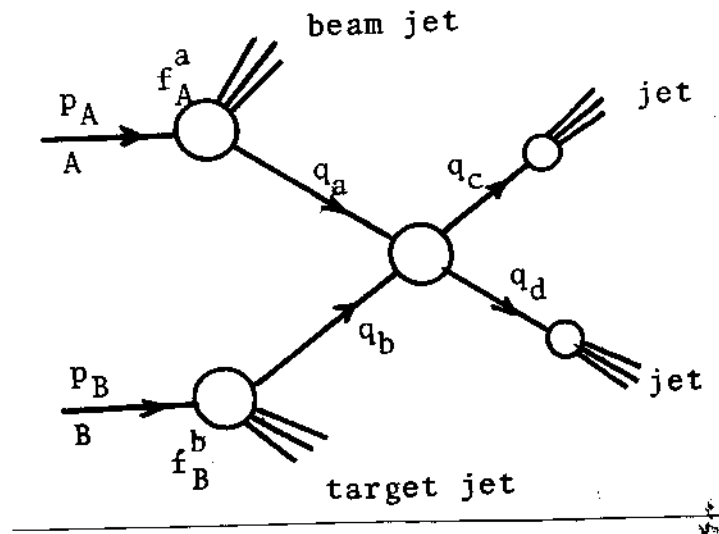
The evolution equations (5.10) and (5.11) allow us to determine the gluon distribution. The distribution obtained from ν -data is shown here.



6. Large P_T processes in hadron-hadron scattering - jets at the collider

6.1. The general picture

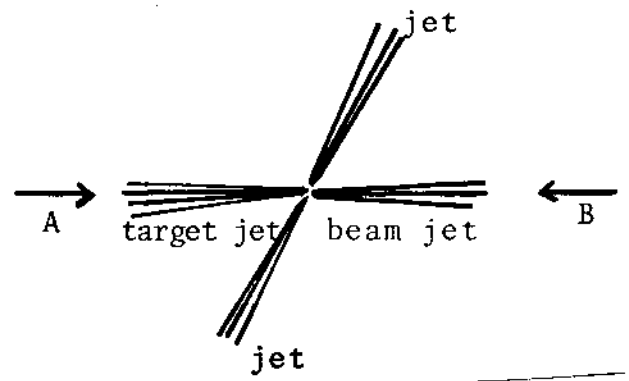
The appearance of jets of hadrons originating from hard scattering of partons is one of the most important predictions of QCD. By hard scattering we mean that the scattered partons have a large angle or a large transverse component. The process is illustrated as:



The incoming particles A and B contain partons a and b which scatter producing partons c and d with large transverse momenta p_T . Partons c and d then fragment into "high p_T " hadron-jets. In the c.m system of A and B we then see the following picture :

Large p_T of partons means that partons have scattered at a small distance ($\sim \frac{1}{p_T}$) thus behaving as point-like particles.

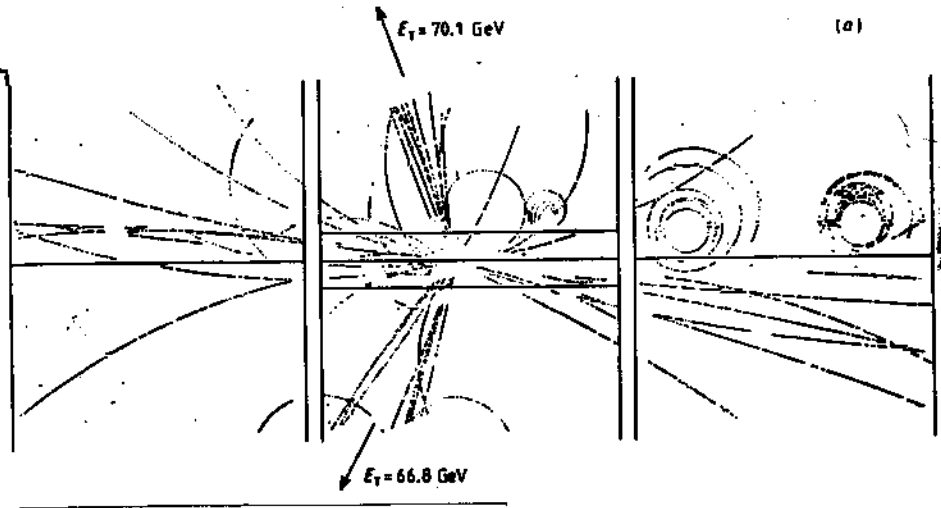
Furthermore it implies that we can apply (perturbative) QCD.



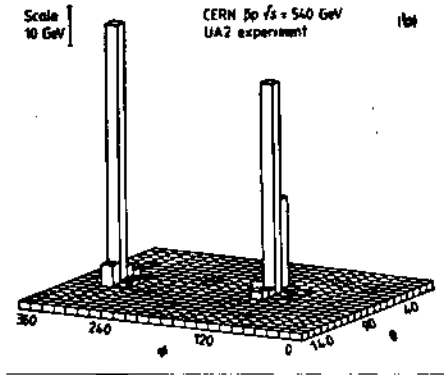
Jets were clearly seen only at the $\bar{p}p$ -collider of CERN at $\sqrt{s} = 540\text{GeV}$

where the total transverse energy ΣE_T (perpendicular to beam axis) is very high.

Jet events observed by the UA1 and UA2 collaborations at CERN. Diagram (a) shows the particle



tracks as reconstructed in the UA1 central detector. Plot (b) corresponds to a two-jet event observed by the UA2 collaboration and shows the transverse energy deposited in the UA2 detector as a function of the polar angle θ and azimuth ϕ .



6.2 Basic mechanism

For our discussion let us introduce the following variables for the parton subprocess:

$$\hat{s} \equiv (q_a + q_b)^2 = (x_1 p_A + x_2 p_B)^2 \approx 2x_1 x_2 p_A p_B \approx x_1 x_2 s$$

where $s = (p_A + p_B)^2 \approx 2p_A p_B$, $x_1 = q_a/p_A$ and $x_2 = q_b/p_B$

$$\hat{t} \equiv (q_a - q_c)^2$$

$$\hat{u} \equiv (q_a - q_d)^2$$

Here masses have been neglected.

The cross section for producing a parton jet of momentum \vec{p}_c and energy E_c in the process

$$AB \rightarrow (\text{jet})_c X$$

can be written as:

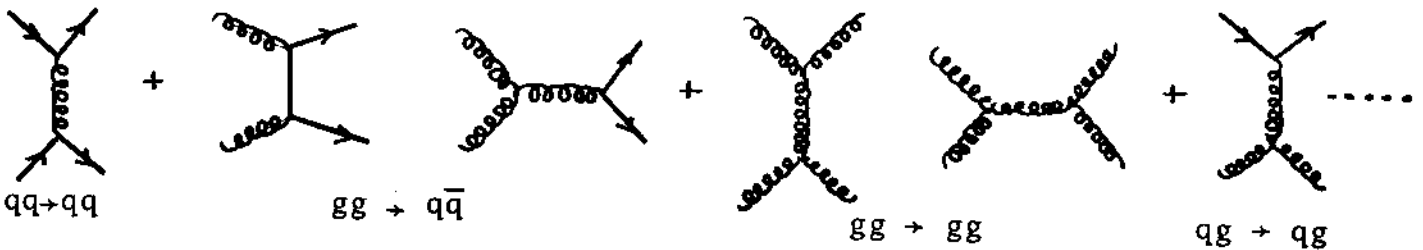
$$E_c \frac{d^3\sigma}{d^3p_c} = \sum_{ab} \int_0^1 dx_1 \int_0^1 dx_2 f_A^a(x_1, Q^2) f_B^b(x_2, Q^2) \left(\frac{E_c d^3\sigma}{d^3p_c} (ab \rightarrow cd) \right) =$$

$$= \sum_{ab} \int_0^1 dx_1 \int_0^1 dx_2 f_A^a(x_1, Q^2) f_B^b(x_2, Q^2) \frac{1}{\pi} \frac{d\sigma}{d\hat{t}} (ab \rightarrow cd)$$

$$\text{with } \hat{s} + \hat{t} + \hat{u} = 0$$

Here $f_A^a(x_1, Q^2), f_B^b(x_2, Q^2)$ are again the structure functions giving the distribution of parton a or b in hadron A or B, respectively.

Some basic QCD diagrams for the subprocess $ab \rightarrow cd$ are the following ones:



The parton cross sections

$$\frac{d\sigma}{d\hat{t}} = \pi \alpha_s^2(Q^2) |M|^2 / \hat{s}^2$$

are shown in table I.

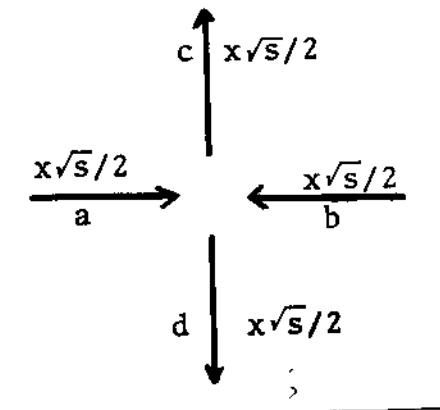
Table I - Parton cross sections: $d\sigma/dt = (\pi\alpha_s^2/s^2) |M|^2$ [averaged (summed) over initial (final) colours and spins]. s, t, u refer to the parton processes.

| PARTON PROCESS | $ M ^2$ |
|--|--|
| $qq' \rightarrow qq'$ $qq' \rightarrow qq'$ | $\frac{4}{9} \frac{s^2+u^2}{t^2}$ |
| $qq \rightarrow qq$ | $\frac{4}{9} \left(\frac{s^2+u^2}{t^2} + \frac{s^2+t^2}{u^2} \right) - \frac{8}{27} \frac{u^2}{st}$ |
| $q\bar{q} \rightarrow q'q'$ | $\frac{4}{9} \frac{t^2+u^2}{s^2}$ |
| $q\bar{q} \rightarrow q\bar{q}$ | $\frac{4}{9} \left(\frac{s^2+u^2}{t^2} + \frac{t^2+u^2}{s^2} \right) - \frac{8}{27} \frac{u^2}{st}$ |
| $q\bar{q} \rightarrow gg$ | $\frac{32}{27} \frac{u^2+t^2}{ut} - \frac{8}{3} \frac{u^2+t^2}{s^2}$ |
| $gg \rightarrow q\bar{q}$ | $\frac{1}{6} \frac{u^2+t^2}{ut} - \frac{3}{8} \frac{u^2+t^2}{s^2}$ |
| $qg \rightarrow qg$ | $-\frac{4}{9} \frac{u^2+s^2}{us} + \frac{u^2+s^2}{t^2}$ |
| $gg \rightarrow gg$ | $\frac{9}{2} \left(3 - \frac{ut}{s^2} - \frac{us}{t^2} - \frac{st}{u^2} \right)$ |

Q^2 should be $\sim p_T^2$. In practice Q^2 is often taken as

$$Q^2 = \frac{2\hat{s}\hat{t}\hat{u}}{\hat{s}^2 + \hat{t}^2 + \hat{u}^2}$$

. In order to see what happens at collider energies let us consider central production where $x_1 \approx x_2 \approx x$ and where the partons are scattered at 90° to the beam axis. We have then the following configuration



This implies that $p_T (=E_T)$ of the scattered parton c or d is

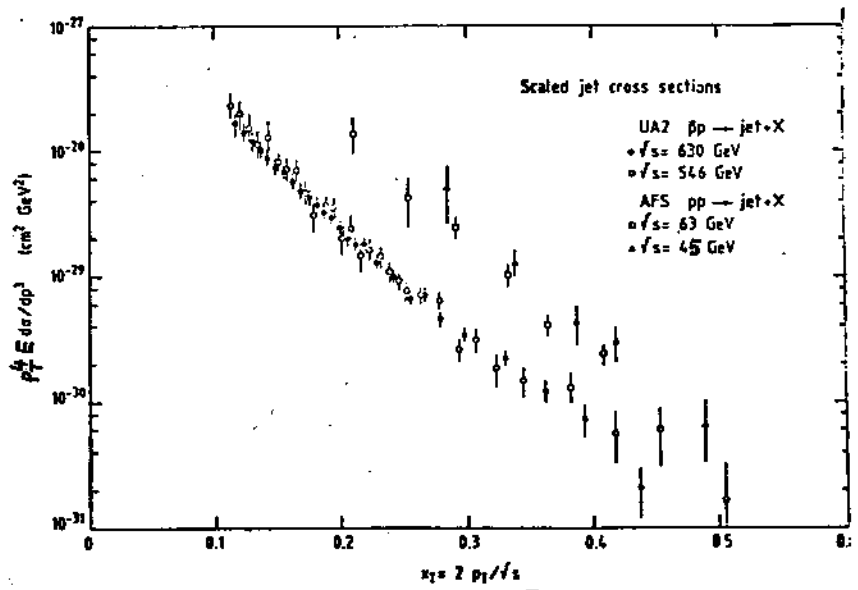
$$p_T = E_T = x\sqrt{s}/2$$

and $\hat{s} \approx x^2s$ and $\hat{t} \approx -\frac{1}{2} x^2s = -2p_T^2$

It is convenient to introduce $x_T \equiv 2p_T/\sqrt{s}$ (i.e. $x_T = x$ for 90° scattering). Since $\sqrt{s} = 540$ GeV at the collider, for $p_T \geq 10 \div 20$ GeV x_T is rather small ($x_T < 0,075$). We already know from deep inelastic scattering that at small x there are many gluons in the nucleon. Moreover the gluon-gluon-gluon coupling is favoured by the colour factors (see also below). We therefore expect the gluon jets to dominate. (This was not the case in the ISR energy range ($\sqrt{s}=63$ GeV) where for $p_T = 20$ GeV $\rightarrow x \approx 0,6$, i.e., in the region of valence quarks (not many). Therefore the cross section is smaller).

- First we see that as long as the structure functions $f_{A,B}^{a,b}(x_{1,2})$ scale, i.e., depend only on x_1 and x_2 we expect at fixed x_T (or fixed angle)

$$\frac{d\sigma}{dp_T^2} = \frac{1}{p_T^4} f(x_T, \alpha_s(p_T^2))$$



Comparison of ISR and $\bar{p}p$ collider data giving clear evidence for scaling violation, i.e., $f_{A,B}^{a,b}(x_{1,2}, Q^2)$.

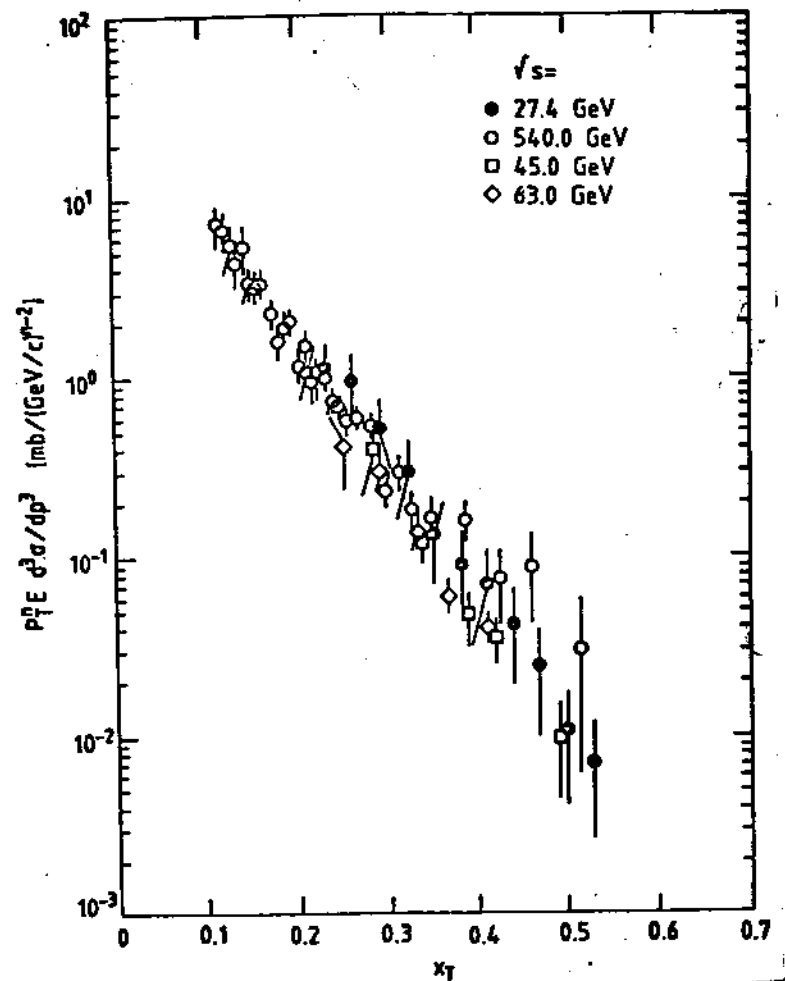
- A good fit to the data ($\sqrt{s} = 27 \rightarrow 540$ GeV) is given by:

$$A = (1,6 \pm 0,3) \times 10^{-26} \text{ cm}^2/\text{GeV}^{2-n}$$

$$n = 5,1 \pm 0,3$$

$$m = 10,6 \pm 0,5$$

with $E \frac{d^3\sigma}{dp^3} = A p_T^{-n} (1-x_T)^m$



6.3. Angular distribution

As we shall see, it offers a test of the vector nature of gluons and the existence of the 3 gluon vertex.

All graphs where there is one-gluon exchange will yield a dependence:

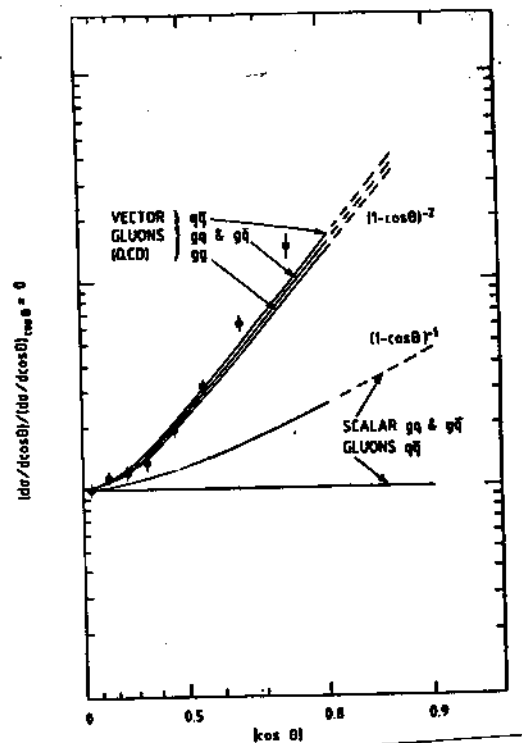
-45-

$$\frac{d\sigma}{d\cos\theta} \sim \frac{1}{(1-\cos\theta)^2} \sim (\sin^2 \frac{\theta}{2})^{-1}$$

as present in the Rutherford formula (Coulomb singularity). Here θ is the scattering angle of the parton subprocess in the C.M. parton subsystem. This angle is equal to the jet-beam angle in the large p_T jets rest frame, provided that the intrinsic momentum of partons in the nucleon and fragmentation effects are neglected. In the subprocesses $qg \rightarrow qg$ and $gg \rightarrow gg$ it arises from the three gluon vertex while in $q\bar{q} \rightarrow q\bar{q}$ it would be present in the Abelian case as well. Fortunately, the angular distribution of all subprocesses listed in Table I are very similar as seen in the figure here:

The data agree with a $(1-\cos\theta)^{-2}$ behaviour thus demonstrating beautifully the vector nature of gluons. They also prove that quarks are point-like particles down to a distance of about 5×10^{-17} cm.

For a better description of the angular distribution, QCD corrections have to be taken into account.



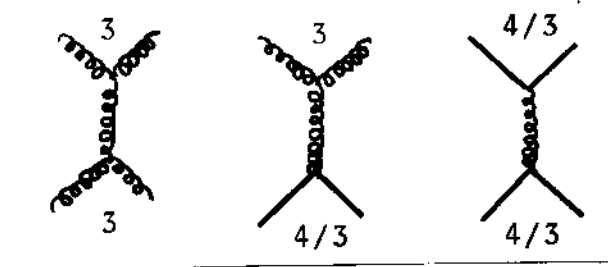
The jet angular distribution (data from UA1).

6.4. Structure functions, factorization

Due to the qqg and ggg couplings, we have approximately

$$(gg + gg) : (qg + qg) : (\bar{q}g + \bar{q}g) : (q\bar{q} + q\bar{q}) =$$

$$1 : \frac{4}{9} : \frac{4}{9} : \left(\frac{4}{9}\right)^2$$

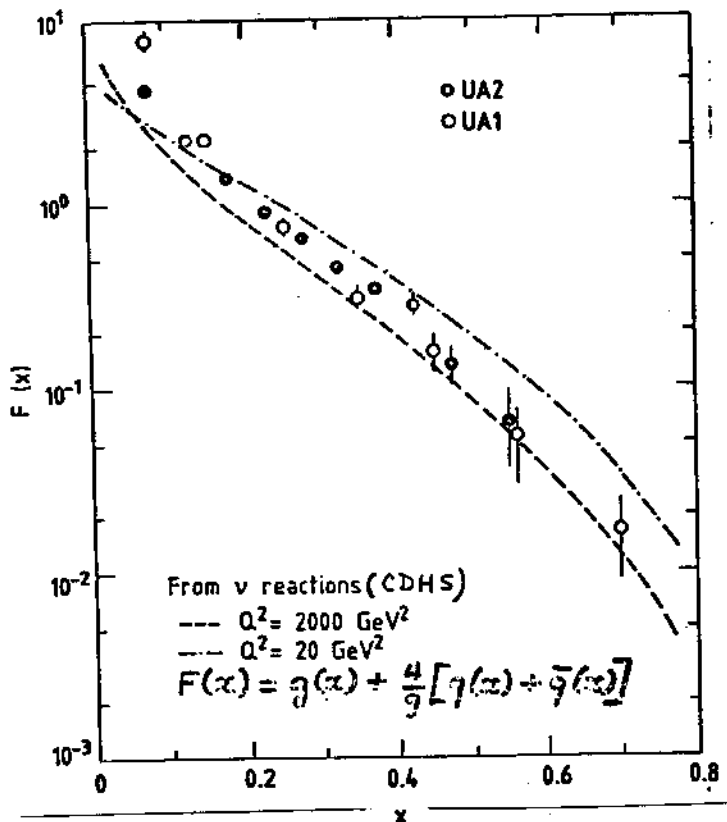


We therefore see a weighted mixture of quark and gluons in the nucleon:

$$F(x) = g(x) + \frac{4}{9} [q(x) + \bar{q}(x)]$$

We then write

$$\frac{d^3\sigma}{dx_1 dx_2 d(\cos\theta)} \approx \left(\frac{d\sigma}{d\cos\theta}\right)_{gg \rightarrow gg} \frac{F(x_1)}{x_1} \frac{F(x_2)}{x_2}$$



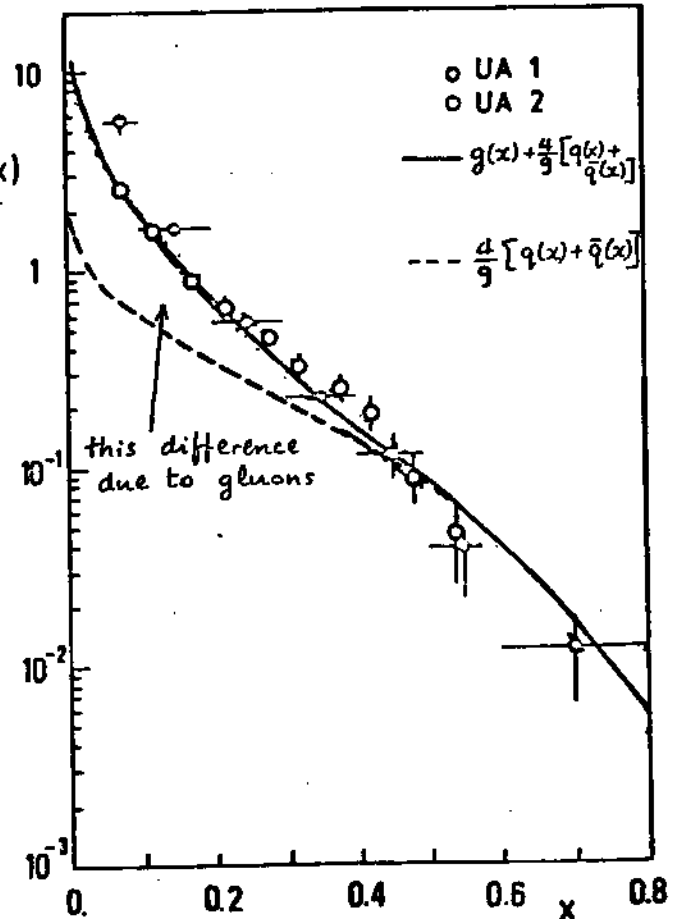
Assumptions: $K = 1$ ($F(x)\sqrt{K}$ is actually measured)

$$\alpha_s(Q^2) = 12\pi/23 \ln(Q^2/\Lambda^2), \Lambda = 0,2 \text{ GeV}$$

Comparison with structure functions measured by CHARM collaboration and extrapolated to $Q^2 \approx 2.000 \text{ GeV}^2$,

This is actually the first direct measurement of the gluon density because in deep inelastic scattering the $g(x)$ is determined indirectly from the Q^2 dependence of $q(x)$ and $\bar{q}(x)$ (Altarelli - Parisi equations).

At the collider one has even observed 3 jet configurations (besides the beam and target jet) as resulting from gluon radiation. From the ratio (3 jets/2 jets) one could extract a value for $\alpha_s = 0,162 \pm 0,024$.

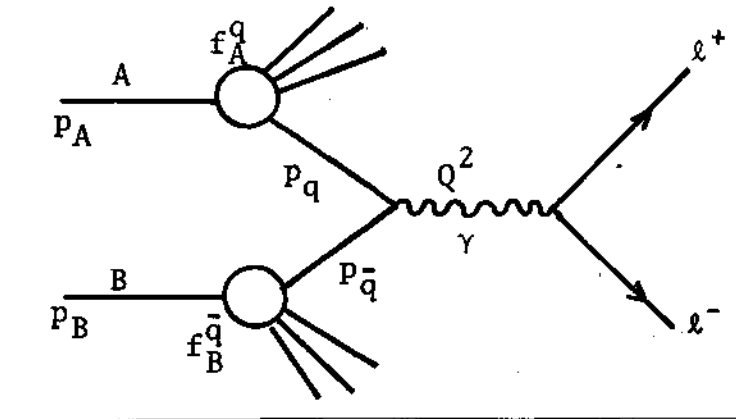


7. Drell-Yan process

Another application of the quark picture and QCD is the Drell-Yan process

$$A + B \rightarrow \ell^+ \ell^- X$$

that is high mass lepton pair production:



The elementary process is $q\bar{q} \rightarrow \mu^+ \mu^-$ which we already know

$$\hat{\sigma}(q\bar{q} \rightarrow \ell^+ \ell^-) = \frac{4\pi\alpha^2}{3Q^2} e_q^2$$

or

$$\frac{d\hat{\sigma}}{dQ^2} = \frac{4\pi\alpha^2}{3Q^2} e_q^2 \delta(Q^2 - \hat{s})$$

where $\hat{s} = (p_q + p_{\bar{q}})^2 = 2p_q p_{\bar{q}} = 2x_1 x_2 p_A p_B = x_1 x_2 s$,

$$s = (p_A + p_B)^2$$

We therefore have

$$\frac{d\sigma}{dQ^2}(AB \rightarrow \ell^+ \ell^- X) = \frac{1}{3} \left(\frac{4\pi\alpha^2}{3Q^2} \right) \sum_q e_q^2 \int_0^1 dx_1 dx_2 \cdot [f_A^q(x_1) f_B^{\bar{q}}(x_2) + f_A^{\bar{q}}(x_1) f_B^q(x_2)] \delta(Q^2 - x_1 x_2 s)$$

(7.1)

The factor 1/3 accounts for the fact that coloured quarks have to form a colour singlet photon. (The $q\bar{q}$ pair must have the same colour. Only 3 $q\bar{q}$ combinations out of 9 are possible).

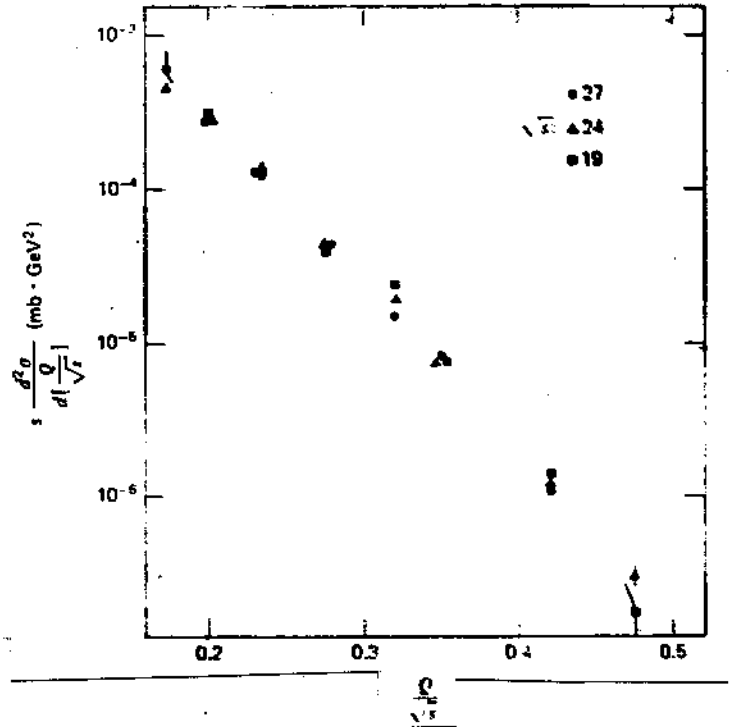
- From eq. (7.1) we obtain the scaling behaviour:

$$Q^4 \frac{d\sigma}{dQ^2} = F(\tau) \quad \text{with} \quad \tau \equiv Q^2/s$$

The following figure shows that the data fulfill this scaling law to a rather good approximation. We also expect the cross

sections for $\pi^+N, K^-N, \bar{P}N$ (for production of high mass $\ell^+\ell^-$ pairs) to be higher than those for PN or K^+N scattering because in the latter two reactions the antiquarks can only come from the sea. This is also seen in the data.

Furthermore one has



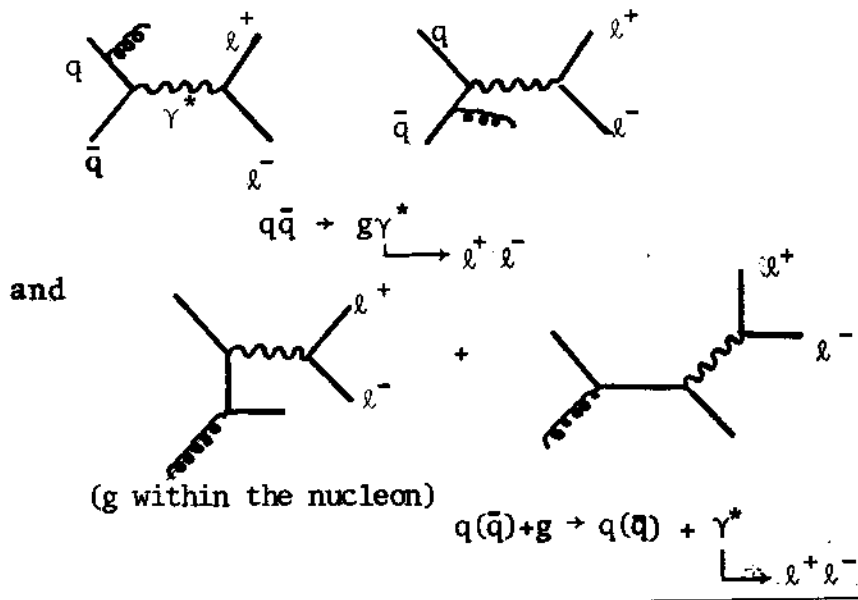
$$\frac{\pi^+N(\text{isoscalar})}{\pi^-N(\text{isoscalar})} = \frac{\frac{1}{9} d\bar{d} + \dots}{\frac{4}{9} u\bar{u} + \dots} \sim \frac{1}{4}$$

The Drell-Yan process $\pi N \rightarrow \ell^+\ell^-X$ also allows a determination of the structure functions for the pion. For instance, NA3 at CERN measured the valence distribution to be

$$x V_{\pi}(x) \sim x^{0,4} (1-x)^{0,9 \pm 0,06}$$

7.1. QCD-effects

In addition to $q\bar{q} + \gamma^* \rightarrow \mu^+\mu^-$ (sec. 7) , also the following processes appear:



(In addition there are virtual gluon corrections).

Taking into account these processes one gets (to leading order) the same formula as above (eq. (7.1)) but the structure functions are replaced by the Q^2 dependent structure functions (as known from deep inelastic lepton hadron scattering) and an overall factor K. This factor should properly account for $O(\alpha_s)$ corrections: besides that $f_{A,B}^{q,\bar{q}}(x) \rightarrow f_{A,B}^{q,\bar{q}}(x, Q^2)$. K should be of the order $1 \div 2,5$.

It can be easily seen by looking at the graphs that by gluon radiation the $\mu^+\mu^-$ pair gets a transverse momentum. It can be calculated to be (at fixed τ)

$$\langle p_T \rangle \cong \alpha_s(Q^2) \sqrt{s} f(\tau, \alpha_s(Q^2)) + \text{const.}$$

where the constant term contains non-perturbative effects (intrinsic k_T of the partons within the nucleon, etc.). The rising of p_T with \sqrt{s} has been seen in the data.

8. W-Z Physics

8.1. W-Z Production

The W and Z production in $p\bar{p}$ collisions goes via the Drell-Yan mechanism just discussed.

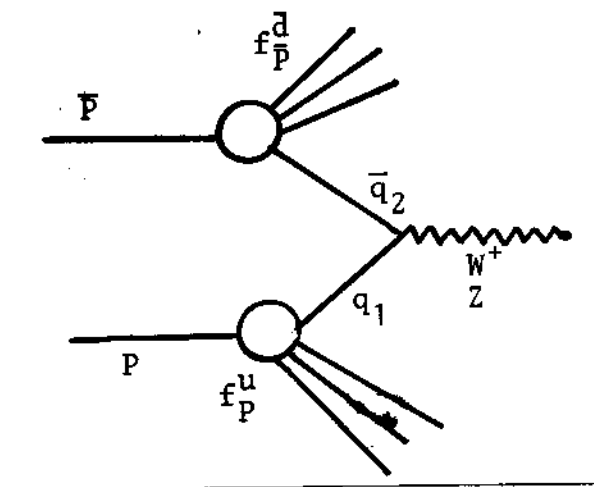
Without taking into account QCD effects for the moment, the elementary subprocesses $q_1 + \bar{q}_2 \rightarrow W$ are:

$$u + \bar{d} \rightarrow W^+$$

$$d + \bar{u} \rightarrow W^-$$

$$u + \bar{u} \rightarrow Z^0$$

$$d + \bar{d} \rightarrow Z^0$$



In analogy to eq. (7.1) we have for the cross section

$$\sigma(p\bar{p} \rightarrow W^+ + \text{anything}) = \int_0^1 dx_1 \int_0^1 dx_2 \hat{\sigma}(x_1, x_2) W^+(x_1, x_2)$$

where $\hat{\sigma}(x_1, x_2)$ is the cross section for the subprocess $q_1 + \bar{q}_2 \rightarrow W^+$ (neglecting the width of the W)

$$\hat{\sigma}(x_1, x_2) = \sqrt{2} G \pi M_W^2 \delta(x_1 x_2 s - M_W^2)$$

with $G \approx 10^{-5} M_p^{-2}$ being the Fermi constant and M_W the W mass.

$W^+(x_1, x_2)$ is the appropriate combination of structure functions

$$W^+(x_1, x_2) = \frac{1}{3} \{ [u(x_1)\bar{d}(x_2) + \bar{d}(x_1)u(x_2)] \cos^2 \theta_c +$$

$$[u(x_1)\bar{s}(x_2) + \bar{s}(x_1)u(x_2)] \} \sin^2 \theta_c$$

The factor $\frac{1}{3}$ has the same origin as explained in section 7. θ_c is

the Cabibbo angle. By making use of the δ -function one can write the cross section in the form:

$$\sigma(\bar{p}p \rightarrow W^+ + \text{anything}) = \sqrt{2} \pi G_F \tau \int_{\tau}^1 \frac{dx}{x} W^+(x, \frac{\tau}{x}) \quad \text{with } \tau = M_W^2/s$$

The cross section for Z^0 production reads:

$$\sigma(\bar{p}p \rightarrow Z^0 + \text{anything}) = 2G_F \sqrt{2} \tau \int_{\tau}^1 \frac{dx}{x} Z(x, \frac{\tau}{x})$$

with $Z = \frac{1}{3} \{ [u(x_1)\bar{u}(x_2) + \bar{u}(x_1)u(x_2)] (\frac{1}{4} - \frac{2}{3} s_w^2 + \frac{8}{9} s_w^4) + [d(x_1)\bar{d}(x_2) + \bar{d}(x_1)d(x_2) + s(x_1)\bar{s}(x_2) + \bar{s}(x_1)s(x_2)] \times (\frac{1}{4} - \frac{1}{3} s_w^2 + \frac{2}{9} s_w^4) \}$,

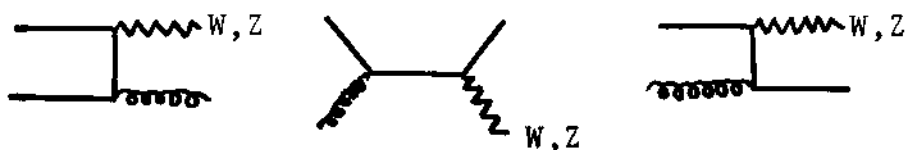
$s_w = \sin^2 \theta_w$ (Weinberg angle)
 $\approx 0,22$

The expressions in the brackets containing s_w correspond to the coupling of the Z^0 to up and down quarks given by the Weinberg-Salam model. The charm distribution in the nucleon has been neglected. Using Q^2 -dependent structure functions one obtains at $\sqrt{s} = 540$ GeV

$$\sigma(W^+) = \sigma(W^-) = 1,8 \times 10^{-33} \text{ cm}^2$$

$$\sigma(Z^0) \approx 10^{-33} \text{ cm}^2$$

Including the next-to-leading order diagrams (see section 7.1) such as

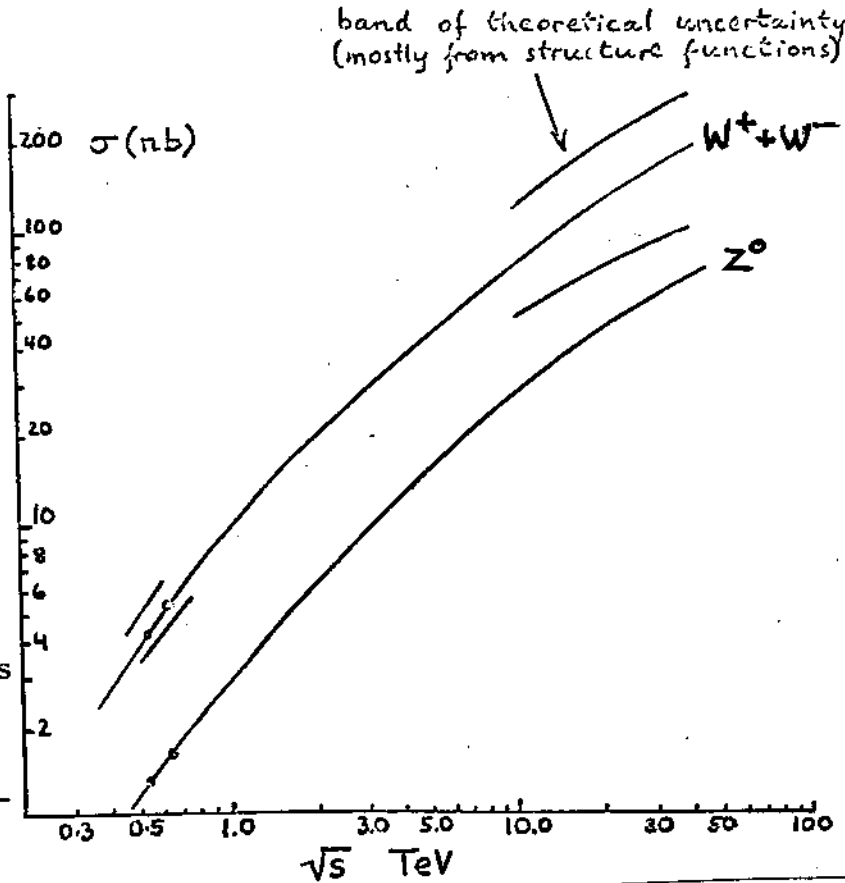


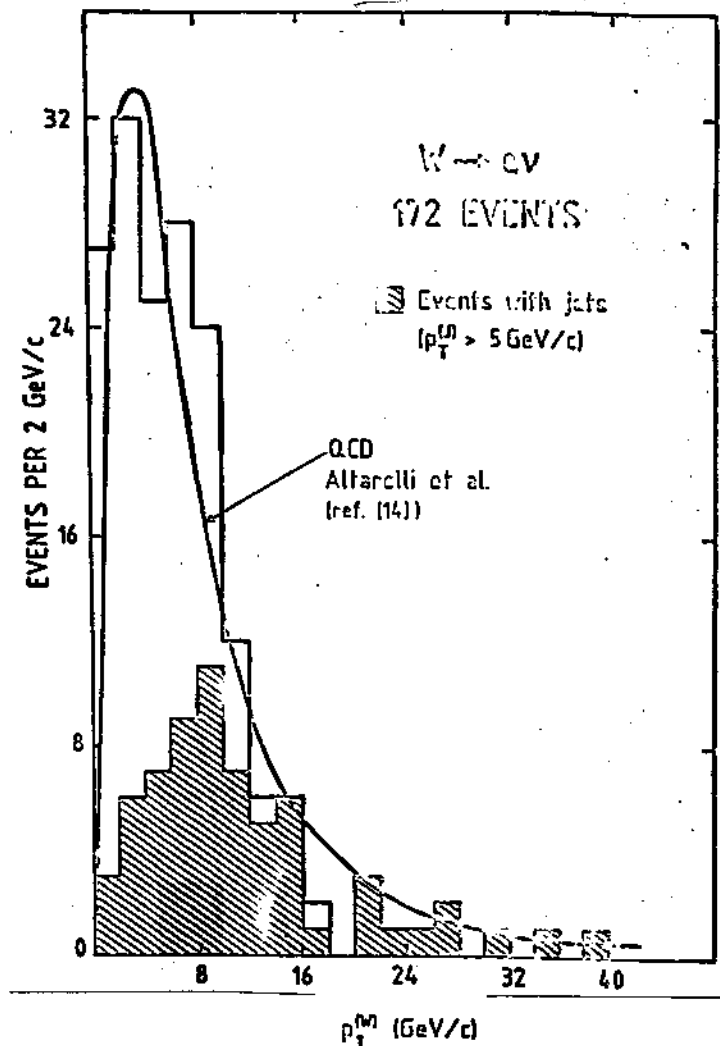
the cross section is expected to be corrected by an overall factor $K \sim 1.3$.

A further effect of including gluon radiation is that the W gets a transverse momentum p_T which is zero in the simple Drell-Yan diagram (section 8.1). The calculation is more subtle because one has to take into account multigluon bremsstrahlung emission.

A comparison of theory and experiment is shown here.

One gets an average p_T of the W :
 $\langle p_T \rangle \approx 7$ GeV. Moreover due to gluon emission one expects $W+1$ (and 2) jet(s) events to be seen.

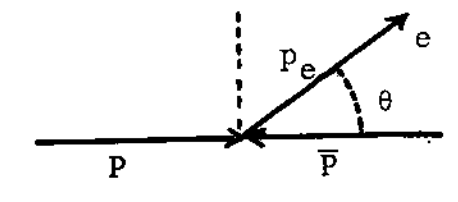




8.2. Detection of $W \rightarrow e(\mu)+\nu$

Although the leptonic decay modes of the W and Z are rather small ($\Gamma_W(e\nu)/\Gamma_{\text{tot}}^W = 9,2\%$, $\Gamma_Z(e^+e^-)/\Gamma_{\text{tot}}^Z = 3\%$) their signature is very clear.

How the detection is made in the case of W is shown here. Assuming first for simplicity the transverse momentum of the W to be zero ($p_T^W = 0$), i.e. the W moving along the beam axis:



We have:

$$p_T^e = p^e \sin\theta = \frac{M_W}{2} \sin\theta^* \quad (\theta^* = \text{angle with respect to the beam axis in } W \text{ rest frame})$$

This holds due to invariance with respect to boosts along the beam axis.

The p_T^e distribution is then given by:

$$\frac{d\sigma}{dp_T^e} = \frac{d\sigma}{d\cos\theta^*} \left| \frac{d\cos\theta^*}{dp_T^e} \right|$$

$$\cos\theta^* = \sqrt{1 - 4p_T^e{}^2/M_W^2}$$

$$\left| \frac{d\cos\theta^*}{dp_T^e} \right| = \frac{4p_T^e/M_W^2}{\sqrt{1 - 4p_T^e{}^2/M_W^2}}$$

This implies that the p_T^e distribution develops a peak at $p_T^e = M_W/2$ due to the singularity of the Jacobian $\left| \frac{d\cos\theta^*}{dp_T^e} \right|$. In reality it is smeared out by $p_T^W \neq 0$ (+ by Γ_W and energy resolution).

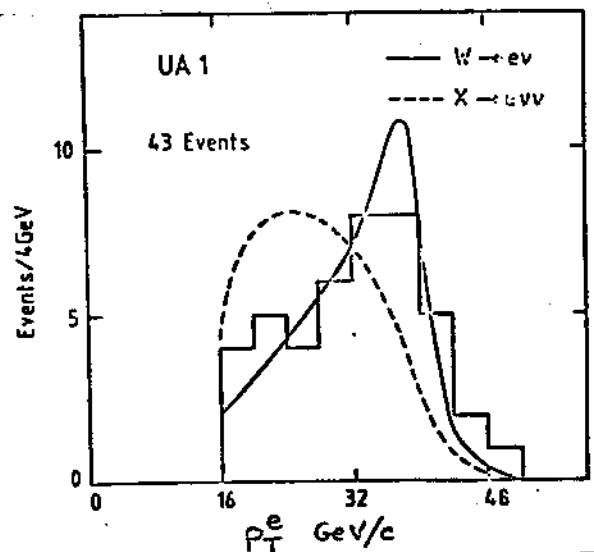
The data show such a behaviour.

To determine the mass M_W of the W one, however, prefers to define a transverse mass $M_T (\leq M_W)$:

$$M_T = (E_T^e + E_T^v)^2 - (\vec{p}_T^e + \vec{p}_T^v)^2 =$$

$$2p_T^e p_T^v (1 - \cos\phi)$$

where ϕ is the angle between \vec{p}_T^e and \vec{p}_T^v , and $\vec{p}_T^v = \vec{p}_T^{\text{miss}}$ is the transverse ν -momentum. This quantity is essentially independent of the W momentum and has a distribution



with a Jacobian peak near $M_T = M_W$.

The following values were obtained:

$$\text{UA1:} \quad M_W = 83,1 + 1,3 \pm 3 \text{ GeV} \\ \quad \quad \quad - 0,8 \\ \quad \quad \quad (\text{stat}) \quad (\text{syst})$$

$$\text{UA2:} \quad M_W = 81,2 \pm 1,1 \pm 1,3 \text{ GeV}$$

For $Z^0 \rightarrow e^+e^-$ there is no problem in determining the mass since both lepton momenta can be measured:

$$\text{UA1:} \quad M_Z = 93,0 \pm 1,6 \pm 3 \text{ GeV} \\ \quad \quad \quad (\text{stat}) \quad (\text{syst.})$$

$$\text{UA2:} \quad M_Z = 92,5 \pm 1,3 \pm 1,5 \text{ GeV}$$

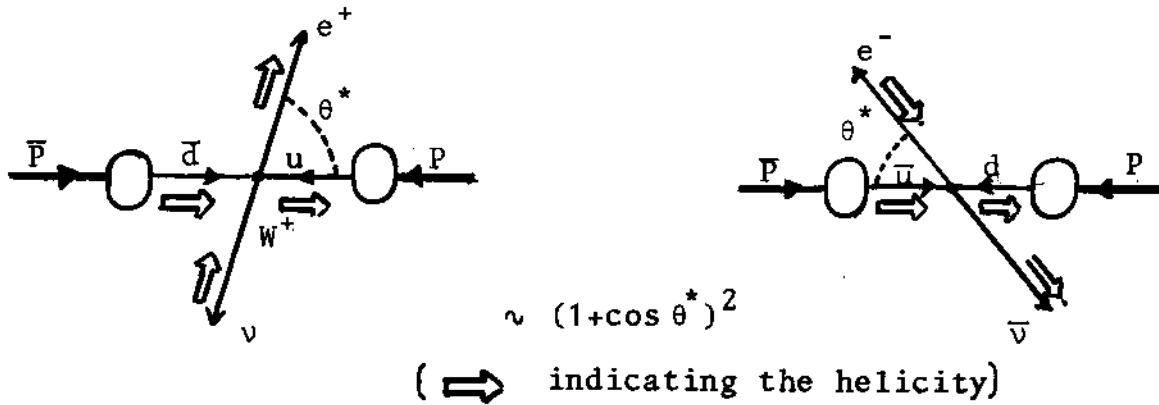
8.3. Charge asymmetry in $W \rightarrow e\nu$

The fact that the W decays weakly due to the V-A coupling in the Standard model is reflected in a charge asymmetry seen in $\bar{p}p$ collisions.

Due to the V-A coupling in the processes

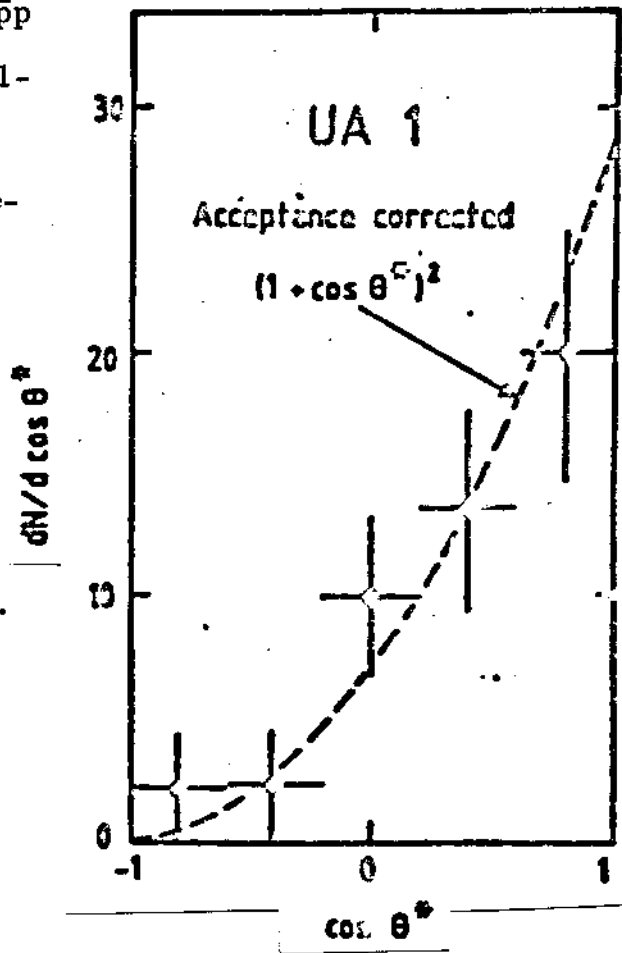
$$u + \bar{d} \rightarrow W^+ \rightarrow e^+ + \nu \\ d + \bar{u} \rightarrow W^- \rightarrow e^- + \bar{\nu}$$

the fermions (e^-, ν, u, d) must have helicity -1 whereas the anti-fermions ($e^+, \bar{\nu}, \bar{u}, \bar{d}$) have helicity +1, i.e., we have the following configuration (in the rest system of the W):



If W production mainly comes from annihilation of valence quarks (which is the case at the CERN $\bar{p}p$ Collider) the e^+ is preferentially emitted along the direction of the antiproton momentum whereas the e^- prefers the proton direction. The data show indeed such a behaviour:

(Note that one would get the same result for the charge asymmetry for a (V+A) coupling).

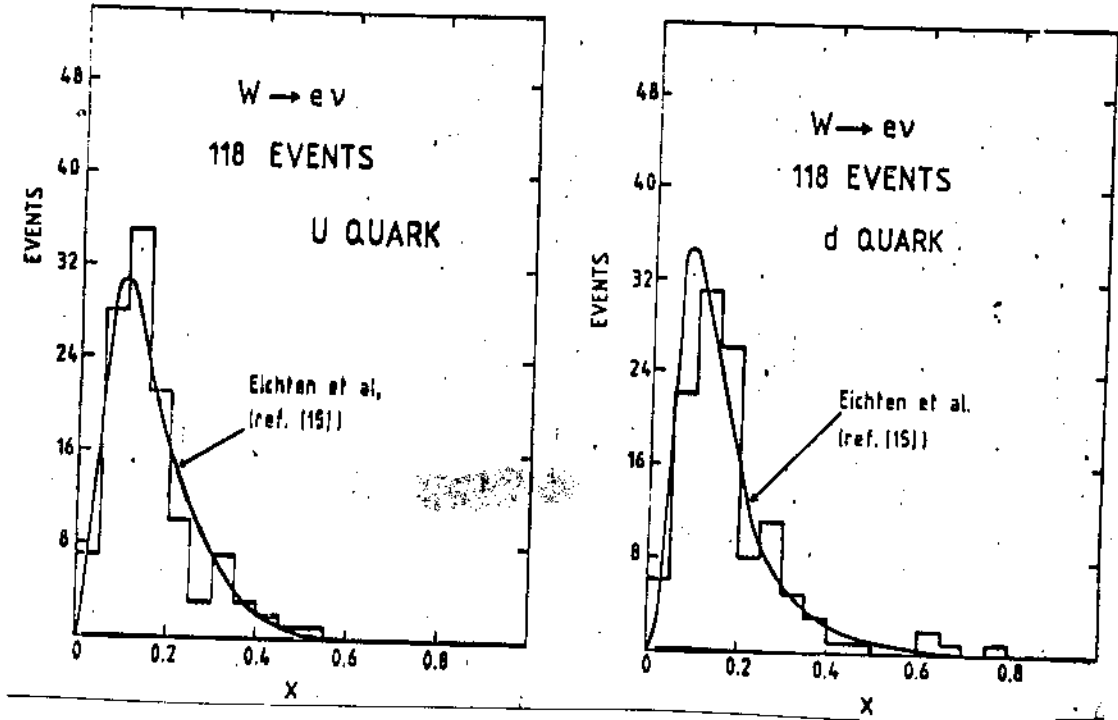


8.4. The quark structure functions

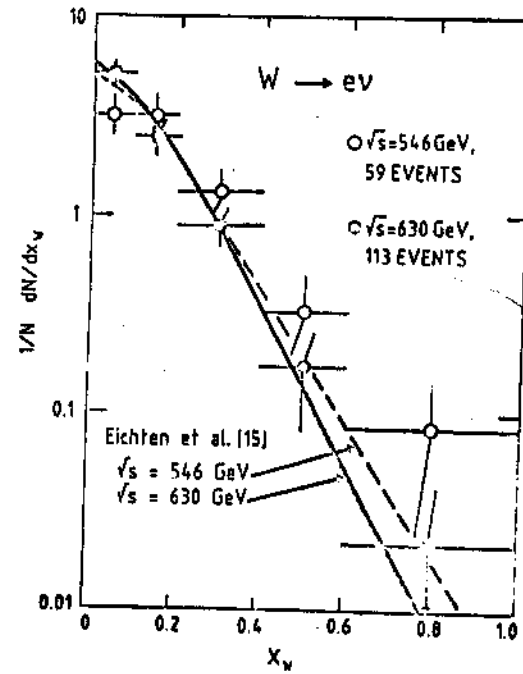
The W-production gives us information about the quark distributions in the proton at $Q^2 = M_W^2$ (see section 8.1). By making use of the relation

$$x_W = \frac{2p_L^W}{\sqrt{s}} = x_1 - x_2, \quad \tau = \frac{M_W^2}{s} = x_1 x_2$$

the UA1 collaboration obtained the following distributions:



The longitudinal momentum distribution of the W is:

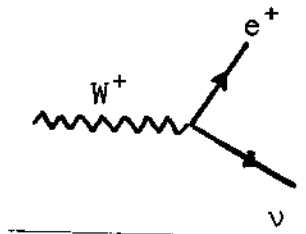


8.5. Comparison with the predictions of the Standard Model

Masses

The Glashow-Weinberg-Salam model yields the relation

$$\frac{G}{\sqrt{2}} = \frac{g^2}{8M_W^2} \quad \text{where } g = e/\sin\theta_W \text{ is the Wev coupling}$$



$$= \frac{ig}{\sqrt{2}} \gamma^\mu \frac{1}{2} (1-\gamma^5) \quad , \quad (8.1)$$

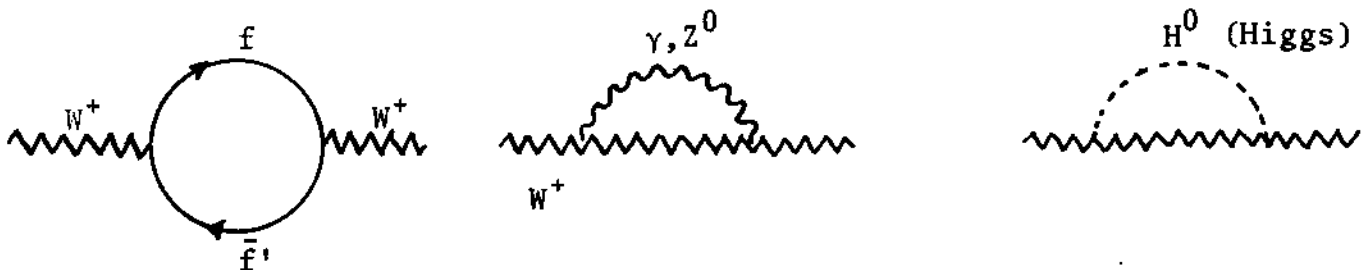
Here θ_W is the Weinberg angle, the Fermi coupling constant

$$G = (1.16638 \pm 0.00002) \times 10^{-5} \text{ GeV}^{-2}, \quad \alpha^{-1} = 137.03604 \pm 0.00011$$

(at $Q^2 = m_e^2$). This leads to

$$M_W = \frac{37.28}{\sin\theta_W} \text{ (GeV)}$$

Radiative corrections like



modify M_W to be

$$M_W = \frac{37.280}{(1-\Delta r)^{1/2}} \times \frac{1}{\sin\theta_W} \text{ (GeV)} \quad (8.2)$$

Δr was calculated (with $m_{\text{top}} = 36 \text{ GeV}$, $M_H \approx M_Z$):

$$\Delta r = 0.0696 \pm \underbrace{0.0020}_{\text{uncertainty in } \sin^2 \theta_W}$$

which gives

$$M_W = \frac{38.65}{\sin \theta_W} \text{ (GeV)} \quad (8.3)$$

(More generally $\Delta r = 0.0696 + \delta$. If, for instance, heavier fermions exist, $m_f \gg 40 \text{ GeV}$, δ would be $\delta = -\frac{3\alpha}{16\pi} \frac{\cos^2 \theta_W}{\sin^4 \theta_W} \frac{m_f^2}{M_W^2} \approx -0.048$ for $m_f = 200 \text{ GeV}$.)

In the case of a heavy Higgs particle $M_H > M_Z$

$$\delta = \frac{11\alpha}{48\pi} \frac{1}{\sin^2 \theta_W} \ln \left(\frac{M_H^2}{M_Z^2} \right) \approx +0.009 \text{ for } M_H = 500 \text{ GeV}$$

Taking the present world average for $\sin^2 \theta_W$ from low energy experiments ($\nu N, \bar{\nu} N, \nu e, \bar{\nu} e$, e (polarized) D, $e^+ e^- \rightarrow \mu^+ \mu^-$)

$$\sin^2 \theta_W = 0.216 \pm 0.006$$

one obtains from eq. (8.3) a mass

$$M_W^{\text{th}} = (83.16 \pm 1.16) \text{ GeV}$$

In the case of the Z^0 we have (within the minimal Higgs scheme)

$$M_Z^{\text{th}} = \frac{M_W}{\cos \theta_W} = \frac{38.65}{\sin \theta_W \cos \theta_W} \quad (8.4)$$

which gives $M_Z^{\text{th}} = (93.92 \pm 1.15) \text{ GeV}$.

These values agree well with the measured masses as given in section 8.2.

- Decays of W and Z

From eq. (8.1) one easily calculates the leptonic partial width of W

$$\Gamma_W(\nu_e e) = \Gamma_W(\mu \nu_\mu) = \Gamma_W(\tau \nu_\tau) = \frac{GM_W^3}{6\pi\sqrt{2}} \approx 250 \text{ MeV} \quad (8.5)$$

For the decay into quarks $q\bar{q}'$ one has to take into account the Kobayashi-Maskawa matrix elements and an extra factor 3 for the 3 colours of the quarks:

$$\Gamma_W(q\bar{q}') = 3 |U_{qq'}|^2 \Gamma_W(\nu e) \quad (8.6)$$

where $U_{qq'}$ is the Kobayashi-Maskawa matrix (see section 1.4).

For $\Gamma_W(t\bar{b})$ we cannot neglect the masses as we did above:

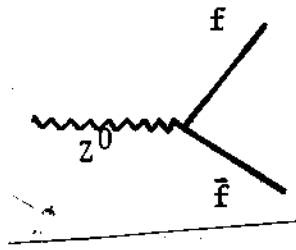
$$\Gamma_W(t\bar{b}) = 3 |U_{tb}|^2 \left(1 - \frac{m_t^2}{M_W^2}\right) \left(1 + \frac{1}{2} \frac{m_t^2}{M_W^2}\right) \Gamma_W(\nu e) \approx 3 \times 0.64 \Gamma_W(\nu e)$$

We therefore have for the total width:

$$\Gamma_W = \underbrace{3\Gamma_W(\nu e)}_{\text{3 lepton doublets}} + \underbrace{(2+0.64) * 3 * \Gamma_W(\nu e)}_{\substack{\text{3 quark} \\ \text{doublets} \\ \uparrow \\ \text{colour}}} \approx 10.9\Gamma_W(\nu e) \approx 2.73 \text{ GeV} \quad (8.7)$$

i.e. the branching ratio $B(\nu e) = \frac{\Gamma_W(\nu e)}{\Gamma_W} = 9.2\%$

In the Weinberg-Salam model, the Z^0 coupling to a fermion-antifermion is:



$$- \frac{ig}{\cos\theta_W} \gamma^\mu \frac{1}{2} (C_V^f - C_A^f \gamma^5)$$

with C_V , C_A as listed in the following table:

| f | C_A^f | C_V^f |
|----------------------------|---------|-------------------------------------|
| ν_e, ν_μ, ν_τ | 1/2 | 1/2 |
| e, μ, τ | -1/2 | $-1/2 + 2 \sin^2\theta_W$ |
| u, c, t | 1/2 | $1/2 - \frac{4}{3} \sin^2\theta_W$ |
| d, s, b | -1/2 | $-1/2 + \frac{2}{3} \sin^2\theta_W$ |

(that is $C_V = I_3^W - 2 \sin^2\theta_W Q$, $C_A = I_3^W$, see section 1.4)

The corresponding widths are therefore

$$\Gamma_Z(\ell\bar{\ell}) = \frac{GM_Z^3}{6\pi\sqrt{2}} [(C_V^\ell)^2 + (C_A^\ell)^2] \quad (8.8)$$

and

$$\Gamma_Z(q\bar{q}) = \frac{GM_Z^3}{6\pi\sqrt{2}} 3[(C_V^q)^2 + (C_A^q)^2]$$

Correcting again for the top mass (assuming $m_t = 40$ GeV), we get

$$\Gamma_Z(t, \bar{t}) \approx 0.25 \Gamma(u\bar{u}).$$

Finally we have:

$$\begin{aligned} \Gamma_Z = & 3[\Gamma_Z(\nu\bar{\nu}) + \Gamma_Z(e^+e^-) + \Gamma_Z(d\bar{d})] + \\ & + 2\Gamma_Z(u\bar{u}) + \Gamma_Z(t\bar{t}) \approx 2.75 \text{ GeV} \end{aligned} \quad (8.9)$$

where in particular for each neutrino one obtains from eq.(8.8)

$$\Gamma_Z(\nu\bar{\nu}) \approx 180 \text{ MeV} \quad (8.10)$$

If there are further neutrino in addition to ν_e, ν_μ, ν_τ with a mass $\ll M_Z/2$, Γ_Z would change according to eq. (8.10)

$$\Gamma_Z = 2.75 + 0.18\Delta N_\nu \text{ (GeV)} \quad (8.11)$$

where ΔN_ν is the additional number of neutrinos. Hence a precise measurement of the total Z^0 -width gives us information on the number of neutrinos and consequently of the particle generations.

- Cross Sections

We already discussed the production cross section of W and Z in section 8.1. Experimentally one could measure

$$\sigma_W^e \equiv \sigma(\bar{p}p \rightarrow W^\pm + \text{anything}) \times B(W \rightarrow e\nu)$$

and

$$\sigma_Z^e \equiv \sigma(\bar{p}p \rightarrow Z^0 + \text{anything}) \times B(Z^0 \rightarrow e^+e^-)$$

The comparison between theory and experiment is shown here

| \sqrt{s} (GeV) | σ_W^e (theory) | UA1 σ_W^e | UA2 σ_W^e |
|---------------------|---|---|----------------------------|
| 546 | 0.36 $\begin{smallmatrix} +0.11 \\ -0.05 \end{smallmatrix}$ | 0.55 \pm 0.08 \pm 0.09 stat syst | 0.49 \pm 0.09 \pm 0.05 |
| 630 | 0.46 $\begin{smallmatrix} +0.14 \\ -0.08 \end{smallmatrix}$ | 0.63 \pm 0.05 \pm 0.09 | 0.53 \pm 0.06 \pm 0.05 |

(σ_W^e is in nanobarns)

| \sqrt{s} (GeV) | σ_Z^e (theory) | UA1 σ_Z^e | UA2 σ_Z^e |
|---------------------|--|---|---------------------|
| 546 | 41 $\begin{smallmatrix} +13 \\ -7 \end{smallmatrix}$ | 40 ± 20 $\begin{smallmatrix} \pm 6 \\ \text{stat syst} \end{smallmatrix}$ | $101 \pm 37 \pm 15$ |
| 630 | 51 $\begin{smallmatrix} +16 \\ -8 \end{smallmatrix}$ | $79 \pm 21 \pm 12$ | $56 \pm 20 \pm 9$ |

(σ_Z^e is in picobarns)

$$\underline{\sin^2 \theta_W}, \quad \rho = M_W^2 / M_Z^2 \cos^2 \theta_W :$$

We can also use eq. (8.3) to calculate the Weinberg angle from the experimental value for M_W (see end of section 4.2) getting:

$$\text{UA1 : } \sin^2 \theta_W = 0.216 \begin{smallmatrix} +0.005 \\ -0.008 \end{smallmatrix} \pm 0.016 \\ \text{syst}$$

$$\text{UA2 : } \sin^2 \theta_W = 0.227 \pm 0.006 \pm 0.007$$

This compares quite well with the world average value from low energy experiments $\sin^2 \theta_W = 0.216 \pm 0.006$.

Furthermore we can determine the parameter $\rho = M_W^2 / M_Z^2 \cos^2 \theta_W$ which (in lowest order) is equal to 1 in the Weinberg-Salam model with the minimum Higgs sector. From the collider experiments one obtains:

$$\text{UA1 : } \rho = 1.018 \pm 0.041 \pm 0.021$$

$$\text{UA2 : } \rho = 0.996 \pm 0.024 \pm 0.009$$

It is often convenient to introduce a "renormalized" definition of

the Weinberg angle (thus being independent of radiative corrections) in terms of physical W and Z masses

$$\sin^2 \theta_W \equiv 1 - \frac{M_W^2}{M_Z^2}$$

Assuming $\rho \approx 1$ one gets from this definition the following values

$$\text{UA1} : \sin^2 \theta_W = 0.202 \pm 0.036$$

$$\text{UA2} : \sin^2 \theta_W = 0.229 \pm 0.03$$

- The Z^0 width Γ_Z and the number of neutrinos

Since a direct measurement of the Z^0 width would require a precise knowledge of the mass resolution, the following method was chosen to determine Γ_Z .

One measures the ratio R of the production cross section for $Z \rightarrow e^+e^-$ over the corresponding one for $W \rightarrow e\nu$:

$$R = \frac{\sigma_Z^e}{\sigma_W^e} = \frac{\sigma(Z) \Gamma_Z(e^+e^-)}{\sigma(W) \Gamma_Z} \cdot \frac{\Gamma_W}{\Gamma_W(e\nu)}$$

where $\sigma(W)$ and $\sigma(Z)$ are the production cross sections for $p\bar{p} \rightarrow W(Z) + X$ (see section 8.1). $\sigma(Z)/\sigma(W)$ is known from QCD being 0.30 ± 0.02 . The ratio $\Gamma_Z(e^+e^-)/\Gamma_W(e\nu)$ can be inferred from the Weinberg-Salam model (see section 8.5). We thus have:

$$\Gamma_W/\Gamma_Z = (9.1 \pm 0.6)R \quad \leftarrow \text{(theoretical uncertainty)}$$

We can furthermore take Γ_W as given by the standard model ($\Gamma_W = 2.73 \pm 0.07$ GeV) and calculate Γ_Z from the measured value $R = 0.125 \pm 0.023$ (average of UA1 and UA2).

By the relation (8.11) one finally obtains an upper bound for the additional number of neutrinos (with masses $\ll M_Z$)

$$\Delta N_\nu < 2.4 \pm 1.0 \quad (90\% \text{ C.L.})$$

Concluding our discussion of e^+e^- , deep inelastic eN reactions, jet production in hadron-hadron collisions and in particular of the properties of production and decay of W and Z in $\bar{p}p$ annihilation we find beautiful agreement with the Standard Model.

This is very satisfying of course. However, we know that the model must be incomplete. Although there are many ideas put forward to extend the model, we have not got any clear hint from experiment in what direction we have to go.

9. Hadronization of quarks and gluons

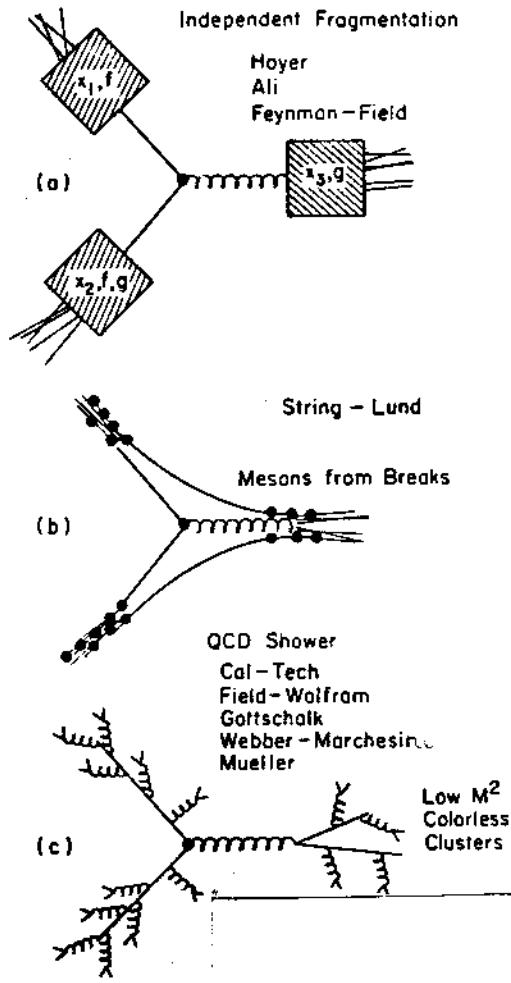
So far we have not yet discussed how (coloured) quarks or gluons fragment into (colourless) hadrons we observe. This mechanism of hadronization is obviously related to the confinement problem not yet fully understood. Although it is not yet possible to calculate the formation of hadron jets from first principles, there has nevertheless been considerable progress in understanding many properties of jets from a phenomenological point of view motivated by QCD.

There are at present three major classes of fragmentation models,

each of which have been implemented in Monte Carlo simulation programs:

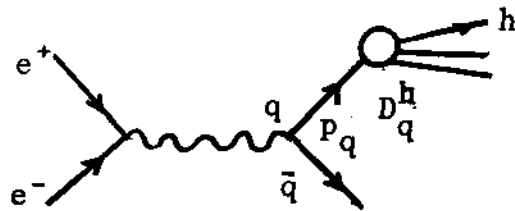
- a) The Independent Fragmentation Model (Feynman-Field model and generalizations)
- b) String Model (Lund model)
- c) QCD-Shower Model

For a 3 jet configuration in the final state of $e^+e^- \rightarrow q\bar{q}g$ they are visualized in the following picture:



9.1. The fragmentation function

Let us first discuss the clearest case $e^+e^- \rightarrow q\bar{q} \rightarrow h+X$



Here the cross section can be written in the form

$$\begin{aligned} \frac{d\sigma}{dz} (e^+e^- \rightarrow hX) &= \sum_q \sigma(e^+e^- \rightarrow q\bar{q}) [D_q^h(z) + D_{\bar{q}}^h(z)] \\ &= \left(\frac{4\pi\alpha^2}{3s}\right) \sum_q e_q^2 [D_q^h(z) + D_{\bar{q}}^h(z)] \end{aligned} \quad (9.1)$$

Here

$$z \equiv \frac{P_h}{P_q} = \frac{P_h}{\sqrt{s}/2}$$

$D_q^h(z)$ therefore is the probability that the hadron h is found in the jet of a quark carrying the fraction z of its energy.

Quite generally, as also in eq. (9.1), it is supposed that the conversion of a parton q into a hadron is independent of how q was produced.

Since the energy of all hadrons fragmenting from a given quark must be the initial energy of the quark, we have

$$\sum_h \int_0^1 z D_q^h(z) dz = 1 \quad (9.2)$$

Moreover the average multiplicity of hadrons of type h is given by

$$\langle n_h \rangle = \sum_{q, \bar{q}} \int_{z_{\min}}^1 D_q^h(z) dz \quad (9.3)$$

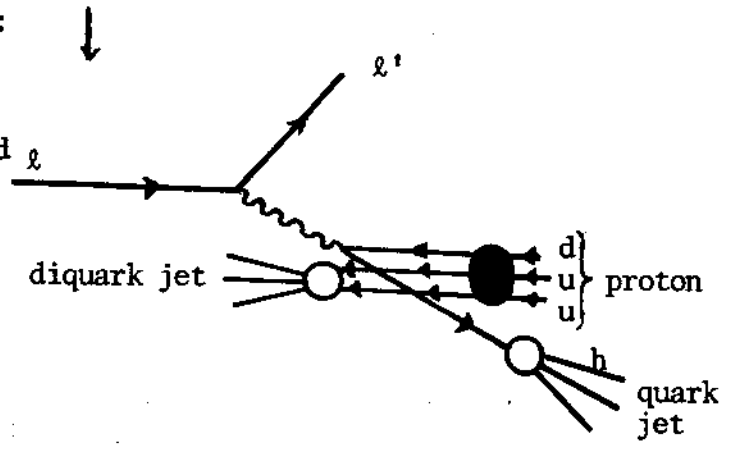
By combining eq. (9.1) and (3.3) one can also

$$\frac{1}{\sigma} \frac{d\sigma}{dz} (e^+e^- \rightarrow hX) = \sum_q e_q^2 \frac{[D_q^h(z) + D_{\bar{q}}^h(z)]}{\sum_q e_q^2} \quad (9.4)$$

(σ is the total cross section)

The quark fragmentation function $D_q^h(z)$ can also be measured in deep inelastic lepton hadron scattering ($\ell N \rightarrow hX$) provided the hadron h is a fragment of the quark q and not of the diquark left over in the nucleon as seen here:

In the centre of mass system the quark jet is equal to the forward jet ($x_F > 0$ or current fragmentation region) whereas the hadrons from the diquark jet lie in the backward region ($x_F < 0$ or target fragmentation region).



It can easily be seen starting from eqs. (5.5), (5.8) and (5.9) that for electro (or muon) production one gets:

$$\frac{1}{\sigma} \frac{d\sigma}{dz} (ep \rightarrow hX) = \sum_q \epsilon_q(x) D_q^h(z) \quad (9.5)$$

where

$$\epsilon_q(x) = \frac{e_q^2 f_N^q(x)}{\sum_q e_q^2 f_N^q(x)}$$

In $\nu(\bar{\nu})$ scattering $\epsilon_d(\epsilon_u)$ is ≈ 1 (with $\cos^2 \theta_c \approx 1$) and all other ϵ_q are small.

Here z is conveniently defined as $z = \frac{p_p^h}{qp} = E^h/v$ (for the definitions see section 5.1).

The fragmentation function can also be expressed as:

$$D^h(z) = \frac{1}{N_{\text{jets}}} \frac{dn^h}{dz} \quad z = \frac{p_L^h}{E_{\text{jet}}} \quad (9.6)$$

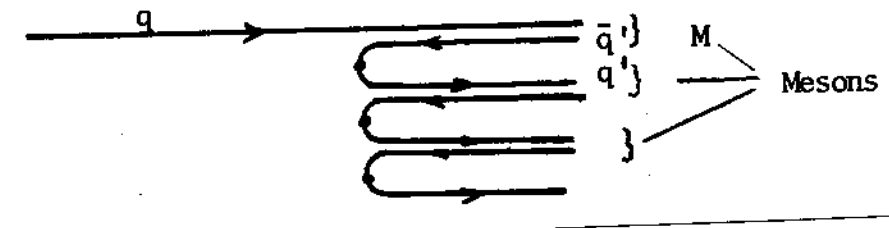
(p_L being the longitudinal momentum component along the jet axis) where N_{jets} is the number of jets and dn^h is the number of particles of type h in the interval dz . This formula is particularly useful in studying jets in hadronic reactions.

9.2. The Independent Fragmentation Model (IFM)

It was originally put forward by Feynman and Field. It describes hadron production in quark jets through the iteration of the fundamental transition

$$q \rightarrow M(q\bar{q}') + q'$$

in which the incident quark fragments into a meson M (containing $q\bar{q}'$) and leaving a quark q' which then undergoes an analogous transition:



If the original quark has four momentum p then each splitting results in a hadron with four-momentum zp and a left-over quark $(1-z)p$. The probability for such a splitting is described by $f(z)$,

-71-

$$f(z) = 1 - a_F + 3a_F(1-z)^2, \quad \int_0^1 dz f(z) = 1 \quad (9.7)$$

where

$$z = \frac{(p_{\parallel} + E)_h}{(p_{\parallel} + E)_q} = \frac{E_h}{E_q}$$

By recursion of this splitting process one can easily derive the following integral equation (typical of cascade pictures) for the fragmentation function of primary hadrons

$$D(z) = f(z) + \int_z^1 d\eta D\left(\frac{z}{\eta}\right) f(1-\eta) \quad (9.8)$$

Corrections for secondary decays of course have to be made when comparing to experiments.

The limited transverse momentum of hadrons within a jet is incorporated into the model by giving the q' and \bar{q}' (in the figure above) a probability distribution

$$\frac{d^2p}{d^2p_T} \sim e^{-p_T^2/2\sigma_q^2}$$

but such that the net transverse momentum of the $\bar{q}' q'$ pair is zero. This guarantees that the transverse momentum of the (primary) hadrons is limited. ($\langle p_T \rangle = \sqrt{\pi} \sigma_q$).

The spin of the produced hadron is determined at each branching by the ratio of vector (ρ, K^*, \dots) to pseudoscalar (π, K, \dots) production by the parameter $\alpha_V = P/P+V$.

The quark-antiquark pairs $\bar{q}' q'$ in the decay chain can be $(u\bar{u}), (d\bar{d})$ or $(s\bar{s})$ with $(u\bar{u})$ and $(d\bar{d})$ produced with equal probabilities. ($c\bar{c}$ production can be neglected). The $s\bar{s}$ production is determined by the parameter γ_S (where $\gamma_S + \gamma_D + \gamma_U = 1$, $\gamma_D = \gamma_U$).

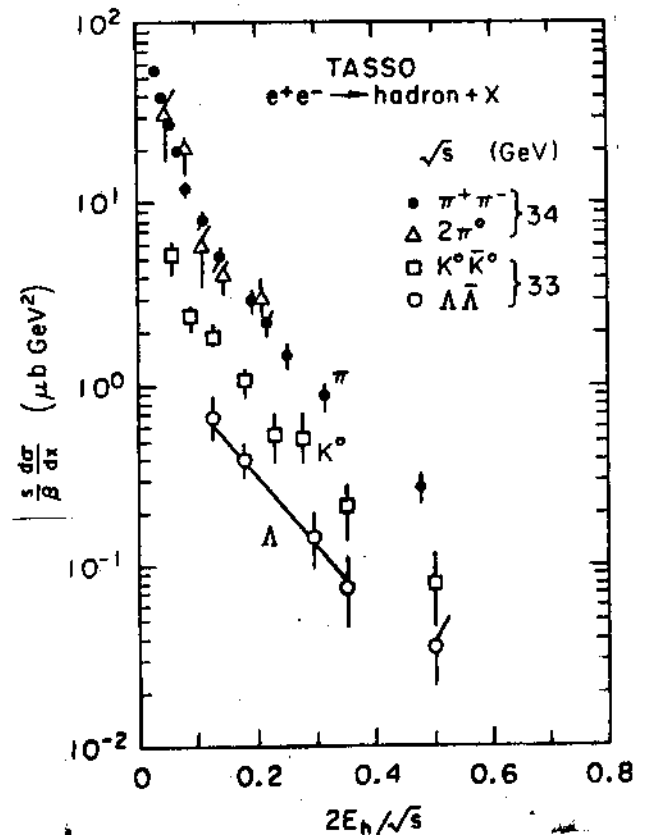
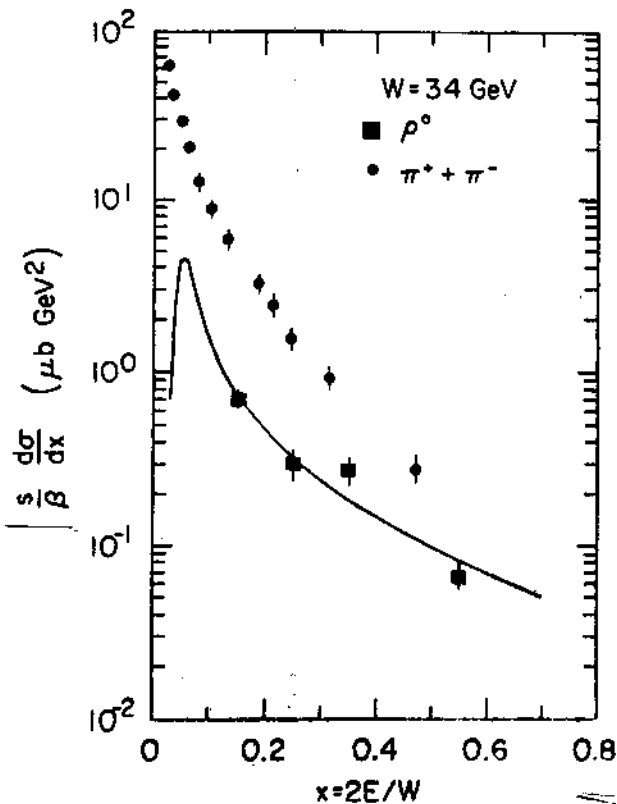
In the Monte Carlo program one does not solve the integral equation (9.8) of course, but starting with a definite quark the particle chain is produced by choosing successively quark-antiquark pairs ($\bar{q}'q'$) according to the probabilities $\gamma_u, \gamma_d, \gamma_s$ and giving the quark q' a momentum according to the probability function $f(z)$. The chain is stopped when the residual quark becomes sufficiently soft. Typically, a minimum value $(E+p_{\parallel})_{\min} \sim 0.5$ GeV is introduced. Unstable vector mesons produced in the chain are then allowed to decay according to the decay modes and branching ratios found in the particle data tables. Values of the parameters in the model were determined by fits to various data: (see the following figures)

$$a_F \approx 0.5 \div 0.7$$

$$\sigma_q \approx 0.32 \div 0.35 \text{ GeV}$$

$$a_V \approx 0.4 \div 0.5$$

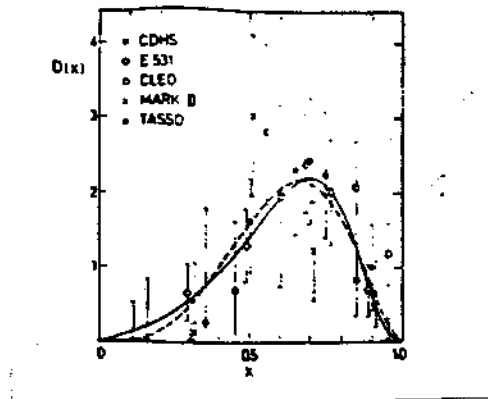
$$\gamma_s \approx 0.17$$



Heavy meson production: Here the heavy quark tends to carry away a large fraction of momentum. In addition, if the production of heavy quark pairs is strongly suppressed, the heavy meson will always contain the primary quark. Therefore the following form is used

$$f_c(z) = \frac{1}{z \left[1 - \frac{1}{z} - \frac{\epsilon}{1-z} \right]^2}$$

where $\epsilon \approx (m_u/m_c)^2 \approx 0.18$ for c quarks and $\epsilon \approx 0.04$ for bottom quarks.



Momentum fraction carried by D^* mesons in c-jet

Also baryon production can be incorporated quite easily by demanding that instead of a quark-antiquark pair a diquark-antidiquark is produced in the chain.

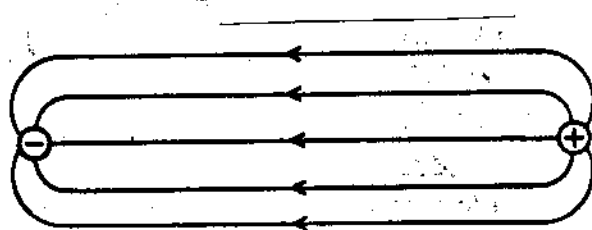
From the ratio of baryon to meson production one can deduce that the probability for this happening is about $0.05 \div 0.1$.

The fragmentation of a gluon can be described by a similar process. The gluon first splits into a quark-antiquark pair. The daughter quark and antiquark then fragment independently, using the scheme described above. The question is only how the energy of the gluon is shared by the quark and antiquark. In one model (Ali) the energy is distributed according to the Altarelli-Parisi splitting function $f_g(z) = z^2 + (1-z)^2$. In another version (Hoyer) either the q or the \bar{q} gets the whole gluon energy with equal probability.

9.3. The Lund String Model

The essential difference between the Independent Fragmentation Model and the String Model concerns the role of confinement. In the string picture independent (isolated) quarks and antiquarks are unphysical. The colour force lines connecting an oppositely coloured quark antiquark pair are supposed to be confined to a narrow tubelike configuration as shown here:

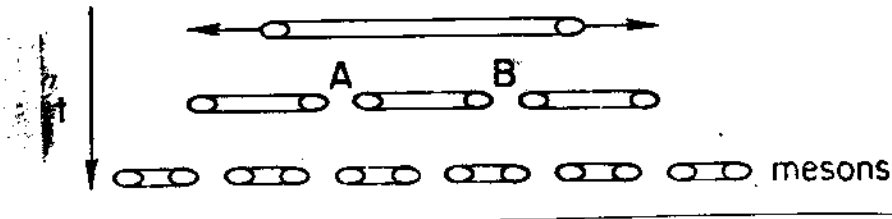
QCD FIELD LINES



Schematic illustrations of field lines between opposite charges in QCD.

From potential models of $q\bar{q}$ bound states we know that the potential energy E between a q and \bar{q} is $E \sim Kd$ where d is the separation between the two quarks and $K \sim 1 \text{ GeV/fm}$ is the string tension. If d increases we will have at some point an energy larger than the mass of two light quarks and have $q\bar{q}$ pair production from the field

between the original pair. The string breaks and forms colourless mesons



In this way the slowest mesons are produced first in contrast to the procedure used in the independent models where fragmentation starts with the fastest quarks. It is therefore called an "inside-out cascade".

In the Lund model a longitudinal fragmentation function of the form

$$f(z) = (1+c)(1-z)^c \approx 0.3 - 0.5 \quad (\text{for } u, d, s \text{ quarks})$$

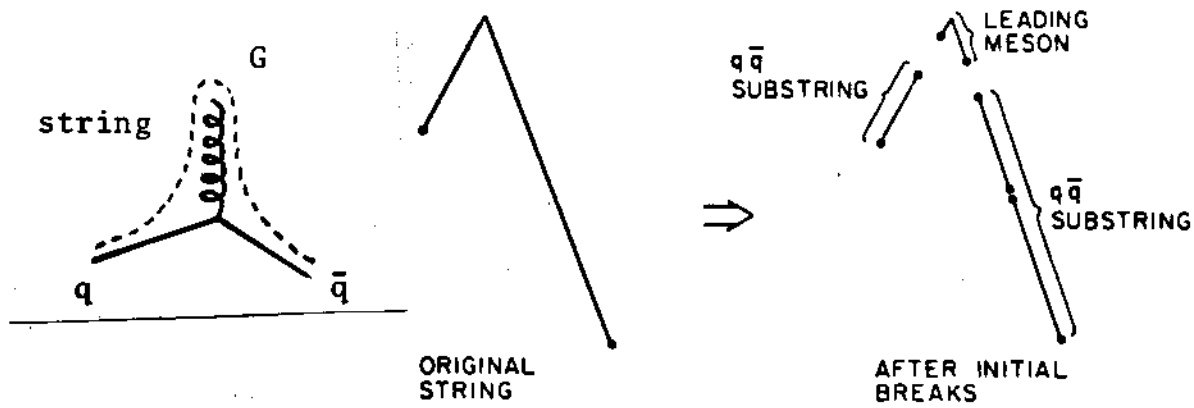
is used. Finite meson mass and transverse momentum relative to the flux tube axis can be understood as a tunneling phenomenon leading to a production probability

$$\sim e^{-\pi(m^2 + p_T^2)/K}$$

thus suppressing strongly heavy quark pair production. Baryon production occurs by occasional creation of a diquark-antidiquark pair during the breaking of the colour string.

Hard gluon emission is added to the model with a probability according to perturbative QCD on the order of α_s (see section 4.2). For a three parton configuration the string is stretched from quark to gluon to antiquark:

HADRONIZATION OF "BENT STRINGS"



Identification of a gluon with a kink in the confining string according to the LUND picture. The kink separates from the string through pair productions in the hadronization picture.

Thus the gluon is identified with a kink in the string. The string breaks at the gluon corner leaving over two $q\bar{q}$ substrings which fragment into hadrons in their own rest frames. Since the gluon energy is shared between the string segments the gluon jet will be softer than a quark jet.

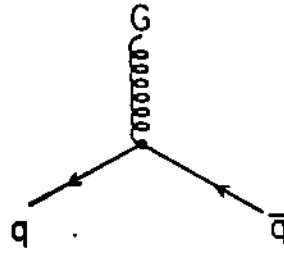
Moreover asymptotically one would have

$$\left(\frac{dN}{dy}\right)_{\text{gluon}} \cong 2 \left(\frac{dN}{dy}\right)_{\text{quark}}$$

A further consequence of this picture is that there are fewer particles produced in the angular region between the q and the \bar{q} than between the quarks and the gluon since particle production occurs along the string.

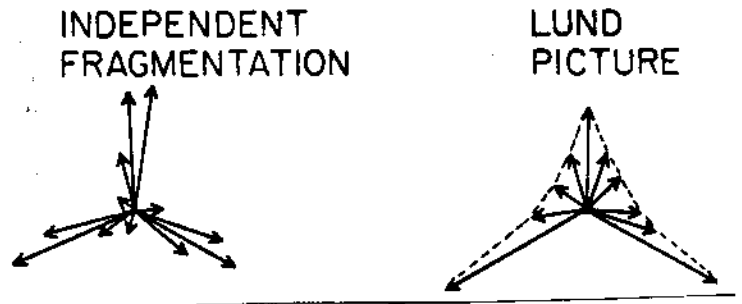
-77-

Schematic illustration of the different topologies for three-jet events expected in the independent fragmentation and LUND pictures.



HADRONIZATION

Adjusting the various parameters of the model it is possible to obtain very good agreement with the experimental data for $\pi^\pm, K^\pm, (p, \bar{p}), (\Lambda, \bar{\Lambda})$ production.

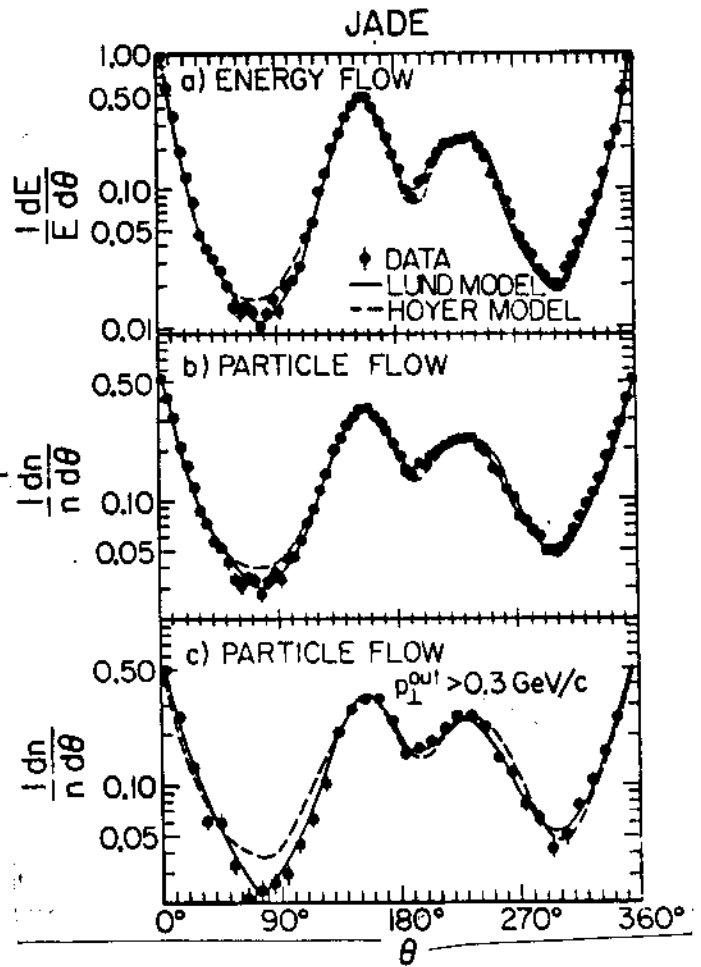


The difference between the

independent fragmentation picture and the Lund String Model is however best seen in "3-jet events", in particular in the angular dependence of the particle and energy flow (the most energetic jet lying along $\theta = 0$).

Here the string model gives a better description than independent fragmentation. In the region between the two "quark jet" peaks, the independent fragmentation prediction is too high. The Lund result is lower in this region since there is no string

Energy and particle flows for 2-jet events in e^+e^- annihilation.



stretching from the quark directly to the antiquark.

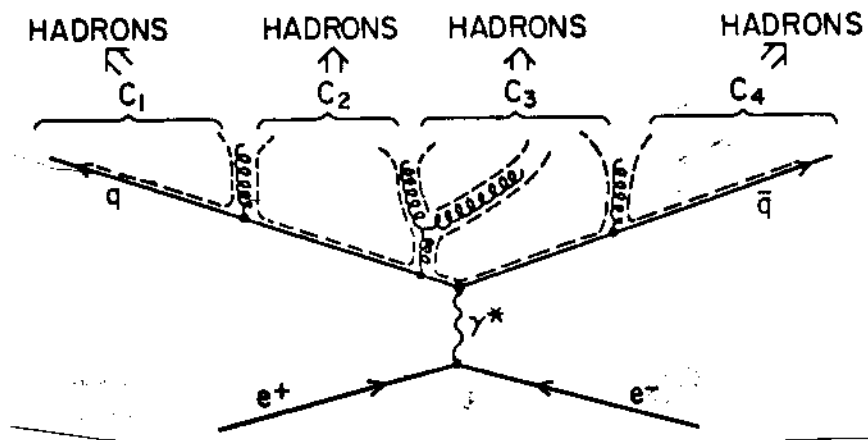
9.4. Parton Shower Models

This class of models is inspired by perturbative QCD. It is best described in the case of $e^+e^- \rightarrow$ hadrons. Hadronization here is essentially a two step process:

- i) Production of a quark gluon shower according to perturbative QCD.
- ii) The formation of light, colour singlet hadronic clusters and independent hadronization of each cluster, mainly isotropic, quasi-two body decay of clusters into known resonances.

It is illustrated in the following picture:

Schematic illustration of the Field-Wolfram model. The dashed lines indicate the strings connecting oppositely colored elements of the parton final state.



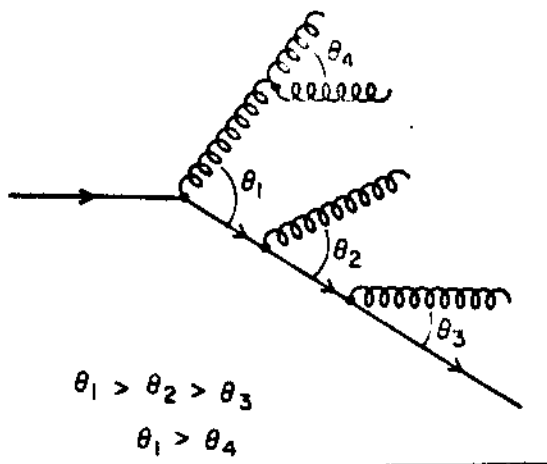
In the initial stages of the evolution all the virtual parton masses are large, $k_i^2 \gg \Lambda^2$ and so, $\alpha_s(k_i^2)$ is small. The diagrams are therefore evaluated according to perturbative QCD, using, for instance, for the branching process $q(p) \rightarrow q(zp) + g((1-z)p)$ the probability function (in the "leading log" approximation): (see section 5.3)

$$dP = \frac{\alpha_s(t)}{2\pi} \frac{dt}{t} dz P_{q \rightarrow q}(z)$$

$$P_{q \rightarrow q}(z) = \frac{4}{3} \frac{1+z^2}{1-z^2}$$

where t is the (off shell) mass of the splitting quark. An analogous formula is valid for the splitting $g \rightarrow gg$ or $g \rightarrow \bar{q}q$. The branching process continues until some lower virtuality scale Q_0 is reached, at which point hadronization (as a non-perturbative mechanism) is supposed to set in. Before forming colour-singlets by quark-antiquark pairs all gluons split into $q\bar{q}$ pairs.

In this class of models no fragmentation functions are used. Besides quark masses and the QCD scale Λ , essentially only one phenomenological parameter is used, the infrared cut-off Q_0 specifying the energy at which one switches from perturbative parton branching to non-perturbative hadronization ($Q_0 \approx 400$ MeV with $\Lambda = 180$ MeV). One point has still to be mentioned which is characteristic of the Webber-Marchesini model. Here the leading infrared singularities are taken into account by ordering successive opening angles.



← Angular ordering of successive radiations in the coherent parton shower formalism.

It implies effectively a coherent treatment of graphs and that soft gluons are correctly taken into account in addition to the collinear

(mass) singularities (see section 4.2).

It is clear that also this model gives no deeper understanding of the non-perturbative part of hadronization (confinement mechanism). However, due to the many ingredients from perturbative QCD (parton shower evolution) and the very small number of parameters it is nowadays the preferred model for comparison with experimental data. The agreement with the data is generally very good.

9.5. Gluon versus Quark Jets

From the discussion above one would expect jets originating from gluons to have a softer energy spectrum, due to enhanced radiation from gluons and the final splitting of a gluon into a quark-antiquark. In QCD the multiplicities of quark and gluon jets behave asymptotically as $\langle N_g \rangle / \langle N_q \rangle \rightarrow 9/4$. Although we may be very far from this region gluon jets should show a higher multiplicity than quark jets. Very recent studies of jets at the $\bar{p}p$ -collider indeed show a softer energy spectrum for gluon jets. There is also an indication that they are less collimated than quark jets and their net charge is consistent with zero.

10. Soft Hadronic Interactions

Hadronic processes at low momentum transfer or small p_T (or soft hadronic interactions) form the bulk of the cross section. Although there is no justification for the use of perturbative QCD in the low p_T regime (there is no large Q^2 or something equivalent) there has been much activity in understanding these processes in a parton framework. We shall here discuss only one approach, the fragmentation approach as implemented in the dual parton model. Quite generally, the motivation for the fragmentation models for soft hadronic processes stems from the surprising similarity between multiparticle production in e^+e^- annihilation, in lepton production and in low p_T hadron-hadron interactions. One calls this universality of fragmentation functions in hard and soft processes.

To illustrate the idea let us consider $pp \rightarrow \pi^+ X$, where the π^+ is produced with a large fraction of the proton momentum. Let us suppose that it comes from the fragmentation of an u quark



This suggests that the cross section should be written in the form:

$$\frac{1}{\sigma} \frac{d\sigma^{p \rightarrow \pi^+}}{dx} = \int_x^1 f_p^u(y) D_u^{\pi^+} \left(\frac{x}{y}\right) \frac{dy}{y}$$

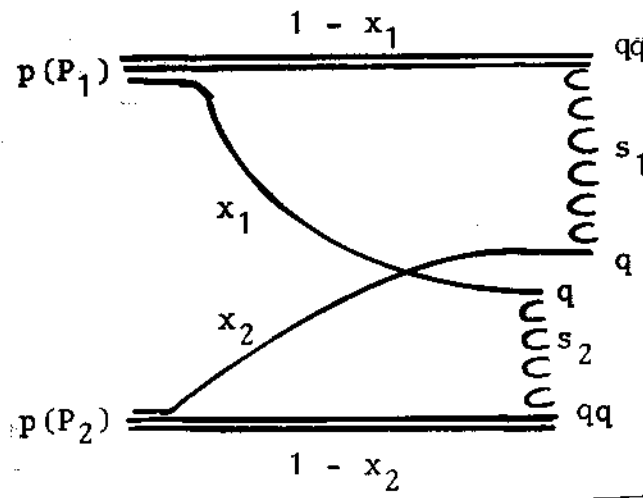
First, it is interesting to observe that with the structure function $f_p^u(x)$ taken from deep inelastic scattering and the known fragmentation function, one would arrive at a result more than an order of magnitude below the data. The reason is quite clear: First, the u quark carries only a fraction of the proton momentum, and second, the π^+ again gets only a part of the u quark momentum. The various models based on the fragmentation mechanism avoid this difficulty by the so-called "held-back" effect. For example, for the meson fragmentation process $\pi^+ p \rightarrow h X$, one valence quark is held back in the central region ($x \approx 0$) and the other valence quark fragments as if it carried all the π^+ momentum. We thus have

$$\frac{1}{\sigma} \frac{d\sigma^{\pi^+ \rightarrow h}}{dx} \approx \frac{1}{2} [D_u^h(x) + D_d^h(x)]$$

since there are equal probabilities for the u or \bar{d} to fragment. Meson fragmentation data are found to compare well with the predictions obtained using the quark fragmentation function from deep

inelastic lepton production data.

Let us now describe in more detail how this held back effect is realized in the dual parton model. The reaction is assumed to be a two step process: colour separation and subsequent fragmentation. For definiteness, we consider the following diagram for pp scattering:



Each proton splits by the interaction into a colour and an anticolour object, i.e., into a quark with momentum fraction x_1 or x_2 and a diquark with momentum fraction $(1-x_1)$ or $(1-x_2)$. Then two chains are formed, each of these between the quark of one proton and the diquark of the other. This is the dominant diagram in the so-called dual topological expansion. It corresponds to Pomeron exchange in the Regge language.

The probability distribution $\rho(x_1, x_2)$ for x_1 and x_2 is taken to be proportional to the valence quark structure functions in a proton

$$\rho(x_1, x_2) = \frac{v(x_1)v(x_2)}{\int_0^1 \int_0^1 dx_1 dx_2 \bar{v}(x_1)\bar{v}(x_2)} = \frac{1}{9} v(x_1)v(x_2)$$

Since the structure functions are peaked at $x \sim 0$, $v(x) \sim x^{-1/2}$ (see

-83-

section 5.2.1), the quarks are "held back" near $x_1, x_2 \sim 0$.

If the total pp centre of mass energy is \sqrt{s} it is easy to see that the chain 1 has the energy

$$s_1 = (p_{qq} + p_q)^2 = [(1-x_1)P_1 + x_2 P_2]^2 \approx s(1-x_1)x_2$$

and correspondingly the chain 2

$$s_2 = s x_1 (1-x_2)$$

The Lorentz boost from the overall CM frame to the CM of chain 1(2) is:

$$\beta_1 = \frac{(1-x_1)-x_2}{(1-x_1)+x_2}, \quad \beta_2 = \frac{x_1-(1-x_2)}{x_1+(1-x_2)}$$

This yields a rapidity shift

$$\Delta_1 = \frac{1}{2} \ln \frac{(1+\beta_1)}{(1-\beta_1)} = \frac{1}{2} \ln \frac{1-x_1}{x_2}$$

$$\Delta_2 = \frac{1}{2} \ln \frac{x_1}{(1-x_2)}$$

The single particle inclusive cross section for $pp \rightarrow hX$ can then be expressed as a superposition of chains 1 and 2:

$$\frac{1}{\sigma} \frac{d\sigma^{pp \rightarrow hX}}{dy} \equiv \frac{dN^{pp \rightarrow hX}}{dy} = \int_q \int_0^1 dx_1 dx_2 \frac{1}{9} v(x_1) v(x_2) \left\{ \frac{dN_1}{dy} (y - \Delta_1, s_1) + \frac{dN_2}{dy} (y - \Delta_2, s_2) \right\}$$

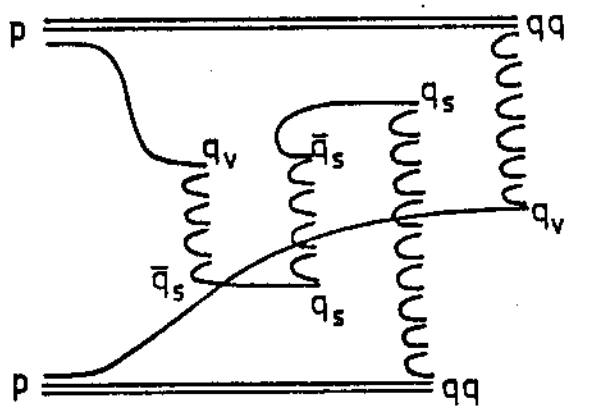
Here dN_1/dy and dN_2/dy are the contributions from the chain 1 and 2, respectively. They can in principle be taken directly from deep inelastic lepton hadron data. They are related to the quark and diquark fragmentation functions in the following way:

$$\frac{dN_1}{dy}(y-\Delta_1, s_1) = \begin{cases} \bar{x}_1 D_{qq}^h(x_1) & , \quad \text{for } y > \Delta_1 \\ \bar{x}_1 D_q^h(x_1) & , \quad \text{for } y < \Delta_1 \end{cases}$$

and correspondingly for dN_2/dy . Here $x_1 = |\mu_\pi \sinh(y-\Delta_1)/0.5\sqrt{s}|$ and $\bar{x}_1 = \sqrt{x_1^2 + 4\mu_\pi^2/s_1}$, $\mu_\pi = 0.33$ GeV (transverse pion mass).

The model as described so far is able to give a qualitative and quantitative understanding of all low p_T multiparticle production data up to ISR energies ($\sqrt{s} \sim 60$ GeV).

Multichain structure: Although the dominant contribution comes from a two chain diagram (Pomeron exchange), with increasing energy the production of new chains (between sea quarks and antiquarks) is energetically possible. They then give additional contributions mainly to the central region. A four chain diagram corresponds in the Regge



← A four chain (two Pomeron) contribution to pp scattering in the dual parton model.

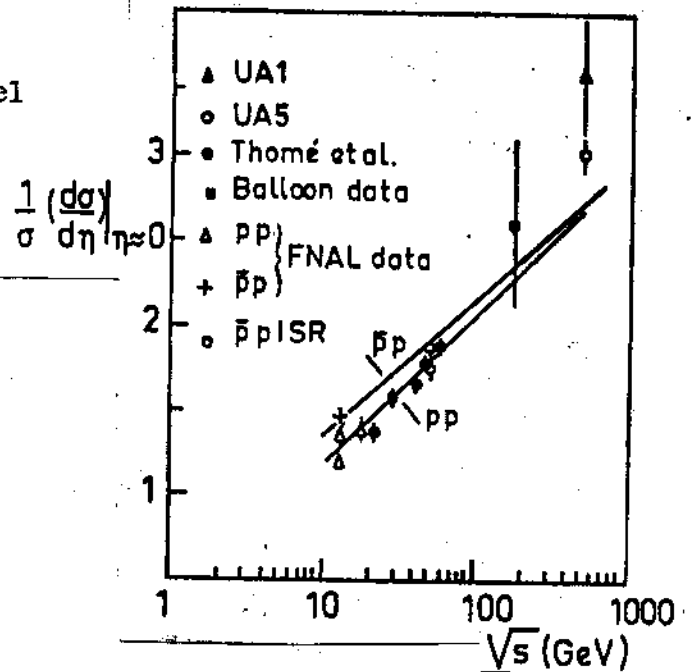
language to two Pomeron exchange.

By including more chains (multiple Pomeron exchange) the model can

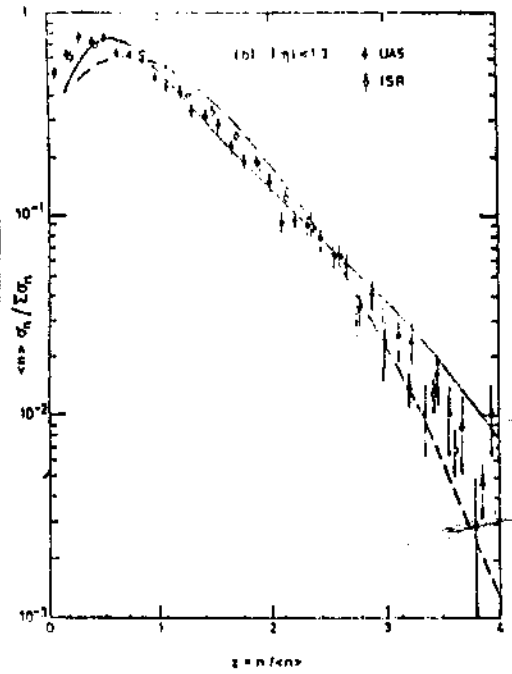
explain the rise of the central rapidity plateau height with energy as observed in going from ISR to SPS collider energies.

-85-

A comparison of the dual parton model with multiple Pomeron exchanges and data on the height of the central rapidity plateau in pp and $\bar{p}p$ collisions.



Furthermore within this model the opening of new chains is also responsible for the violation of the so-called KNO scaling as seen here



Violation of KNO scaling for reduced rapidity interval $|y| < 1.3$.

To summarize, although we are still far from describing soft hadronic processes quantitatively purely within the framework of QCD, considerable progress has been made in interpreting multiparticle production within a quark-parton picture.

ACKNOWLEDGEMENTS

I am very much indebted to Prof. Anna Maria Freire Endler for having given me the opportunity to work here in a very enjoyable atmosphere. I also thank her for the help in preparing these lecture notes.

I want to express my thanks to the Centro Brasileiro de Pesquisas Físicas for the warm hospitality and the financial support I received during my stay here.

I also thank Mrs. Helena de S. Ferreira for the efficient typing of the manuscript.

BIBLIOGRAPHY

We give here a set of monographs and review articles which were used in preparing these lectures.

- P.D.B. Collins and A.D. Martin: Hadron Interactions; Adam Hilger Ltd., Bristol, 1984.
- F. Halzen and A.D. Martin: Quarks and Leptons; John Wiley, 1984.
- Chris Quigg: Gauge Theories of the Strong, Weak and Electromagnetic Interactions; The Benjamin=Cummings Publishing Company, 1983.
- C. Rubbia: Lectures within the 1981-1982 Academic Training Program, CERN.
- L. di Lella: Lectures within the 1984-1985 Academic Training Program, CERN.
- L. di Lella: Physics from the $\bar{p}p$ Collider; invited talk at the Intern. Conf. on High Energy Physics, Bari, Italy, 1985.
- R. Horgan and M. Jacob: Physics at Collider Energy; CERN 81-04, 1981.
- R. Hollebeek: Jets in e^+e^- Annihilation; SLAC-PUB-3242, 1983.
- Th.D. Gottschalk: Hadronization and Fragmentation; CERN-TH-3810, 1984.
- P. Darriulat: The Strong Interaction: Experimental Approaches; CERN-EP/84-152, 1984.
- J. Steinberger: Inclusive Lepton-Hadron Experiments; CERN-EP/84-159, 1984.
- D. Haidt: Experimental Tests of Gauge Theories; DESY 84-108, 1984.
- U.P. Sukhatme: in Proc. of the Multiparticle Dynamics Conf. 1982, p. 718, Volendam, Ed.: W. Kittel, W. Metzger, A. Sterigou; World Scientific Publ. Comp., Singapore.
- A. Capella and J. Tran Thanh Van: in Proc. of the Multiparticle Dynamics Conf. 1984, p. 163, Lund; Ed.: G. Gustafson, C. Peterson; World Scientific Publ., Singapore.
- G. Marchesini and B. Webber: *ibid.*, p. 612 and p. 627.